

# Universal and non-universal features of glassy relaxation in propylene carbonate

W. Götze and Th. Voigtmann

*Physik-Department, Technische Universität München, D-85747 Garching, Germany*

(received ... November 1999)

## Abstract

It is demonstrated that the susceptibility spectra of supercooled propylene carbonate as measured by depolarized-light-scattering, dielectric-loss, and incoherent quasi-elastic neutron-scattering spectroscopy within the GHz window are simultaneously described by the solutions of a two-component schematic model of the mode-coupling theory (MCT) for the evolution of glassy dynamics. It is shown that the universal  $\beta$ -relaxation-scaling laws, dealing with the asymptotic behavior of the MCT solutions, describe the qualitative features of the calculated spectra. But the non-universal corrections to the scaling laws render it impossible to achieve a complete quantitative description using only the leading-order-asymptotic results.

PACS numbers: 64.70.Pf, 61.20.Lc

## I. INTRODUCTION

In this paper the evolution of structural relaxation as observed upon cooling the van-der-Waals liquid propylene carbonate (PC) from above the melting temperature ( $T_m = 218$  K) to the glass-transition temperature ( $T_g = 160$  K) will be analyzed. It will be shown that the spectra, as measured within the four-decade frequency window below 800 GHz by depolarized-light-scattering, by dielectric-loss, and by neutron-scattering spectroscopy can be quantitatively described by the solutions of a two-component schematic model of the mode-coupling theory (MCT), where the drift of the various spectral features over several orders of magnitude due to temperature changes can be fitted by smooth variations of the model parameters. The results of the data fits will be used to demonstrate in detail which features can be explained by the universal  $\beta$ -relaxation-scaling laws of the asymptotic MCT-bifurcation dynamics, and which are caused by either preasymptotic corrections to this scaling or by crossover phenomena to microscopic oscillatory motion.

Glassy PC spectra within the full GHz window have first been studied by Du et al. [1] using depolarized-light-scattering spectroscopy. It was shown that the data can be interpreted with the universal laws predicted by MCT. In its basic version, which is also referred to as the idealized MCT, this theory implies an ideal liquid-glass transition at a characteristic temperature  $T_c$ . In an extended version,  $T_c$  marks a crossover from the high-temperature regime, where the dynamics is dominated by non-linear-interaction effects between density fluctuations, to a low-temperature regime, where the dynamics deals with activated-hopping transport in an effectively frozen system. For temperatures  $T$  near  $T_c$ , the MCT equations can be solved by asymptotic expansions for the so-called  $\beta$ -relaxation regime. This results in formulas for universal features of the MCT dynamics as reflected in the appearance of dynamical scaling laws, power-law-decay processes, and in algebraically diverging time scales. The different anomalous exponents and also the  $\beta$ -relaxation-master functions are determined by a system-dependent number which is called the exponent parameter  $\lambda$  [2]. The data analysis of Ref. [1] suggested  $T_c \approx 187$  K and  $\lambda \approx 0.78$ . Relaxation

curves measured for PC within the pico-second window in solvation-dynamics studies [3] and dielectric-loss spectra determined within the GHz window [4–6] have also been analyzed with the MCT-scaling-law formulas using parameters  $T_c$  and  $\lambda$  consistent within the experimental uncertainties with the values cited above. The critical temperature for PC has first been determined to  $T_c \approx 180$  K [7] by interpreting the  $\alpha$ -relaxation time for density fluctuations measured by neutron-scattering spectroscopy with the MCT-power-law prediction for this quantity. A similar analysis of the viscosity [1,7] suggests a value of  $T_c$  near 190 K. The effective Debye-Waller factor for the elastic modulus has been measured for PC by Brillouin-scattering spectroscopy [8]. Interpreting this quantity with the asymptotic formula of the idealized MCT, a critical temperature considerably higher than 190 K has been suggested. However, since the data interpretation is not compelling [1], this finding cannot be considered to be a falsification of the  $T_c \approx 187$  K result. Thus one could conclude, that MCT describes some essential features of the glassy dynamics of PC qualitatively correct, a statement which also holds for a series of other glass-forming systems [9].

In order to arrive at a more stringent assessment of MCT, Wuttke et al. [10] have re-examined the above cited PC data for  $T > T_c$ . In addition, they have studied incoherent-neutron-scattering spectra  $S(q, \omega)$  for a two-decade window in frequency  $\omega$  and for wave vectors  $q$  between 0.7 and  $2.3 \text{ \AA}^{-1}$ . The data exhibited the predicted factorization in a  $q$ -dependent but  $\omega$ -independent amplitude  $h_q$ , and a  $q$ -independent term describing the frequency and temperature variation:  $S(q, \omega) \propto h_q \chi''(\omega)/\omega$ . The susceptibility spectrum  $\chi''(\omega)$  showed the subtle dependence on  $\omega$  and on  $(T - T_c)$  predicted by the MCT-scaling laws for the  $\beta$ -process, provided  $T_c \approx 182$  K and  $\lambda \approx 0.72$  was chosen. These parameters are marginally compatible with the values found in the above cited earlier work on PC. The depolarized-light-scattering spectra have been remeasured within the  $\beta$ -relaxation window for  $T > T_c$ . The spectrometer used in Ref. [10] incorporated several improvements over the one used in the original study [1], resulting in improved signal-to-noise ratios. Furthermore, the use of a narrow-band interference filter eliminated the possibility of higher-order transmission effects which have recently been recognized as a potential source of artifacts

[11,12]. But the new spectra agree with the old ones within the error bars of the latter. The remeasured spectra could be fitted convincingly with the universal asymptotic results using the newly found values for  $T_c$  and  $\lambda$ . It was shown in addition that also the solvation-dynamics results [3] and the dielectric-loss spectra [4–6] could be fitted within the same frame using the new values for  $T_c$  and  $\lambda$ . Actually, the new fit to the dielectric-loss data [10] is more convincing than the original one [4–6], since the fit interval expands with decreasing  $(T - T_c)$ , as requested by MCT. The size of the  $(T - T_c)$  interval and the window for the frequency where leading-order-asymptotic results describe the MCT-bifurcation dynamics, depend on the probing variable [13,14]. It was assumed in [10] that the range of validity of the asymptotic analysis is smaller for the dielectric-loss spectra than for the light-scattering spectra. It also had to be anticipated that preasymptotic corrections can account for a 35% offset of the  $\beta$ -relaxation-time scale of the neutron-scattering data relative to the one for the light-scattering data.

To corroborate the cited MCT interpretations of glassy PC spectra, the previous work shall in this paper be extended in three directions. First, the  $\alpha$ -relaxation peaks will be included in the analysis, so that the low-frequency limit for the fit interval can be decreased to 1 GHz or lower. Thereby the crossover from  $\alpha$ - to  $\beta$ -relaxation and the non-universal  $\alpha$ -peak shapes can be described as well. Second, the crossover from relaxation to vibrational dynamics will be included in the analysis, so that the high-frequency limit for the fit interval can be increased by about a factor of four. Third, an extended form of the MCT instead of the idealized one will be used, so that the spectra for depolarized-light scattering and dielectric loss for  $\omega \geq 1$  GHz can be described also for temperatures below  $T_c$ . The specified goals will be achieved by studying the full solutions of an MCT model.

The paper is organized as follows: In Sec. II, the basic formulas for the schematic model to be used will be summarized, and then (Sec. III) the experimental data sets are fitted using this model with smoothly drifting parameters. After a short introduction to the necessary equations for the asymptotic analysis for the model (Sec. IV), the  $\beta$ -scaling laws are tested against the data in Sec. V. In Sec. VI, it will be shown that for the studied model a properly

defined dielectric modulus is more suited for a description by scaling laws than the dielectric function. Section VII presents some conclusions.

## II. A SCHEMATIC MODE-COUPLING-THEORY MODEL

The idealized MCT is based on closed equations of motion for the auto-correlation functions of the density fluctuations  $\phi_q(t)$ , which are positive definite functions of time  $t$ , depending on the wave vector modulus  $q$  [15]. The extended MCT also includes couplings of the density correlators  $\phi_q(t)$  to the auto-correlation functions for the currents [16]. The general equation of motion expresses the density correlator in terms of relaxation kernels. It is formulated most transparently with Laplace-transformed quantities. For the latter, the convention  $F(z) = i \int_0^\infty \exp(izt) F(t) dt$  with complex frequency  $z$ , and  $F(\omega) = F'(\omega) + iF''(\omega)$  for  $z = \omega + i0$  will be used.

$$\phi_q(z) = \frac{-1}{z + C_q(z)}, \quad (1a)$$

$$C_q(z) = N_q(z) - \frac{\Omega_q^2}{z + M_q^{\text{reg}}(z) + \Omega_q^2 m_q(z)}. \quad (1b)$$

Here,  $\Omega_q$  denotes a characteristic frequency given by the thermal velocity  $v$  and the static structure factor  $S_q$ :  $\Omega_q^2 = q^2 v^2 / S_q$ . The general current-flow kernel  $C_q(z)$  describes density-fluctuation decay via two parallel channels. Phonon-assisted hopping is given by  $N_q(z)$ . The relaxation due to nonlinear interactions of density fluctuations is described by a force-fluctuation kernel which consists of a sum of a regular term  $M_q^{\text{reg}}(z)$  and a mode-coupling term  $m_q(z)$ . The former deals with normal-liquid dynamics, and the latter with the slow motion caused by the cage effect. It is obtained as a polynomial  $\mathcal{F}_q$  of the density correlators  $\phi_q(t)$ :

$$m_q(t) = \mathcal{F}_q [\phi_q(t)]. \quad (1c)$$

The coefficients of the polynomial are non-negative; they are given by the equilibrium structure and hence depend smoothly on external control parameters like temperature  $T$ . Systematic studies of the kernels  $N_q(z)$  and  $M_q^{\text{reg}}(z)$  are not available. The theory shall be

simplified by Markov approximations of these quantities:  $M_q^{\text{reg}}(z) = i\nu_q$ ,  $N_q(z) = i\Delta_q$ . The friction constants  $\nu_q \geq 0$  and hopping coefficients  $\Delta_q \geq 0$  shall be treated as model parameters, which depend smoothly on  $T$ .

Equations (1) can exhibit bifurcation singularities. Generically, if as a single control parameter the temperature is considered, the singularity occurs for a critical temperature  $T_c$  if all hopping coefficients  $\Delta_q$  vanish. If some  $\Delta_q \neq 0$ , the singularity is avoided. However, for small  $\Delta_q$  and small  $|T - T_c|$  the singularity causes an anomalous dynamics: the glassy dynamics studied by MCT. At the singularity the correlators do not decay to zero but to a positive value  $f_q^c$ , which is called the plateau. It is approached by an algebraic decay law, called the critical decay, which is specified by an anomalous exponent  $a$ ,  $0 < a \leq 1/2$ :

$$\phi_q(t) - f_q^c = h_q(t/t_0)^{-a} + \mathcal{O}(t^{-2a});$$

$$T = T_c, \quad \Delta_q = 0. \quad (2)$$

The quantity  $h_q > 0$  is called the critical amplitude, and it can be determined from the mode-coupling functional  $\mathcal{F}_q$  for  $T = T_c$ . The time scale  $t_0$  is determined by the transient dynamics for  $T = T_c$ . For  $\Delta_q = 0$  and small but negative  $(T_c - T)$ , the correlator falls below the plateau  $f_q^c$  according to the von Schweidler law  $\phi_q(t) - f_q^c \propto -t^b + \mathcal{O}(t^{2b})$ , characterized by a second anomalous exponent  $b$ ,  $0 < b \leq 1$ . From  $\mathcal{F}_q$  for  $T = T_c$ , one can calculate the above mentioned exponent parameter  $\lambda$ ,  $0 < \lambda \leq 1/2$ , which determines the critical exponent  $a$  and the von Schweidler exponent  $b$  via  $\Gamma(1 - a)^2 / \Gamma(1 - 2a) = \lambda = \Gamma(1 + b)^2 / \Gamma(1 + 2b)$ . In the so-called  $\beta$ -relaxation window, implicitly defined by  $|\phi_q(t) - f_q^c| \ll 1$ , MCT predicts that the dynamics is in leading order controlled by merely two smooth functions of  $T$ : the separation parameter  $\sigma$  and the hopping parameter  $\delta$ . The former is determined by  $\mathcal{F}_q$ , and its zero defines the crossover temperature  $T_c$ :  $\sigma = C(T_c - T)/T_c + \mathcal{O}((T - T_c)^2)$ . The latter obeys  $\delta \geq 0$ ; generically,  $\delta$  vanishes only if  $\Delta_q = 0$  for all  $q$ . The shape of the correlation functions in the asymptotic regime of the  $\beta$ -relaxation window is fully determined by the exponent parameter  $\lambda$ ; as can be inferred from Ref. [2] and the original papers cited therein.

Testing the relevance of MCT by comparing the leading-order results for the  $\beta$ -relaxation

with data is however hampered by a great difficulty. Without detailed microscopic calculations one cannot determine the size of the corrections to the asymptotic formulas, and therefore their range of validity is not known. In addition, the optimal choice of  $\lambda$ , fixing the shape of the  $\log \chi''$ -versus- $\log \omega$  graph is tedious to decide upon and might well depend on the choice of the fit interval. The difficulty of fixing  $\lambda$  from a  $\beta$ -relaxation study alone was demonstrated recently for the hard-sphere system [17]. A set of density correlators  $\phi_q(t)$  calculated for various wave vectors and packing fractions was considered. A fit to them with the asymptotic predictions for a significantly wrong  $\lambda$  was by a standard fitting procedure not distinguishable from the correct fits within typical experimental windows.

A different route for data interpretation is based on comparison of the measured spectra with the complete solutions obtained from schematic MCT models. This procedure was studied first by Alba-Simionescu et al. [18–20]. Schematic models are truncations of the complete set of Eqs. (1) to a set dealing with a small number of correlators only. Thus the mathematical complexity of the problem is reduced considerably. Alas, the connection of the mode-coupling-functional coefficients with the microscopic structure gets lost; the coefficients are to be treated as fit parameters. The main advantage of this approach is that one does not rely on the applicability of asymptotic formulas; one is sure that all results on crossover phenomena and preasymptotic corrections are logically consistent with the MCT.

The simplest schematic model deals with a single correlator only, which shall be denoted by  $\phi(t)$ . The first MCT equation is equivalent to Eqs. (1a,b) with  $q$  indices dropped:

$$\phi(z) = \frac{-1}{z + i\Delta - \Omega^2 / [z + i\nu + \Omega^2 m(z)]} . \quad (3a)$$

For the mode-coupling functional, a quadratic polynomial that can reproduce all valid values for the exponent parameter  $\lambda$  is used [21]:

$$m(t) = v_1 \phi(t) + v_2 (\phi(t))^2 . \quad (3b)$$

For  $\Delta = 0$ , ideal liquid-glass transitions occur on a line in the  $v_1$ - $v_2$  plane of coupling constants. One can use  $\lambda$  to parameterize this line of critical coupling constants:

$$v_1^c = (2\lambda - 1)/\lambda^2, \quad v_2^c = 1/\lambda^2, \quad 1/2 \leq \lambda < 1. \quad (4)$$

Thus this model is specified by two control parameters  $(v_1, v_2)$ , by two frequencies  $(\Omega, \nu)$  quantifying the transient dynamics, and one rate  $\Delta$  for the activated transport processes. The model has many non-generic features, and therefore one cannot expect it to describe a measured spectrum. In the present paper, the correlator  $\phi(t)$  is introduced to mimic in an overall fashion the combined effect of all structure fluctuations in producing the bifurcation point and the exponent parameter  $\lambda$  of the system.

The dynamics of some probing variable  $A$  coupling to density fluctuations shall be described by a second correlator, to be denoted  $\phi_A^s(t)$ . It obeys an equation analogous to Eq. (3a):

$$\phi_A^s(z) = \frac{-1}{z + i\Delta_A^s - \Omega_A^s{}^2 / [z + i\nu_A^s + \Omega_A^s{}^2 m_A^s(z)]}. \quad (5a)$$

Again the microscopic dynamics is quantified by two frequencies referred to as microscopic parameters  $(\Omega_A^s, \nu_A^s)$ . The activated relaxation processes are described by  $\Delta_A^s$ . The mode-coupling functional shall be specified by a coupling to  $\phi(t)$  quantified by a single coupling constant  $v_A^s$ :

$$m_A^s(t) = v_A^s \phi(t) \phi_A^s(t). \quad (5b)$$

It is a peculiarity of this model, that the dynamics of the probing variable  $A$  is influenced by  $\phi(t)$  but not vice versa. Thus the position of the transition is not modified by the introduction of the second correlator nor is the value of  $\lambda$ . The model was motivated by Sjögren [22] for the description of tagged-particle motion in a glassy environment, and it will be used here in the same context for the interpretation of the neutron-scattering data. The MCT for the reorientational dynamics of a non-spherical probe molecule suggests the same schematic model for the dipole and quadrupole relaxation [23]; an observation that motivates the application of the model for the description of the dielectric-loss and depolarized-light-scattering spectra, respectively. For the incoherent-neutron-scattering cross-section the fit will be done using the model parameters for  $\phi_A^s(t)$  different for different wave vectors. For

the index  $A$  the abbreviations ls, de, and ns for light scattering, dielectric loss, and neutron scattering, respectively, will be used. The specified two-component schematic model has been used earlier for data interpretation with the restriction to  $\Delta = \Delta_A^s = 0$ . Depolarized-light-scattering spectra within the full GHz band have been described for glycerol for all temperatures above  $T_g$  [24], and for ortho-terphenyl for  $T > T_c$  [25]. Rufflé et al. [26] were the first to simultaneously describe glassy spectra for several probing variables  $A$ . Within the  $\beta$ -relaxation regime, they fitted coherent-neutron-scattering spectra for several wave vectors and also the longitudinal elastic modulus for  $\text{Na}_{0.5}\text{Li}_{0.5}\text{PO}_3$ .

The single coupling constant  $v_A^s$  determines all features of the structural-relaxation part of the second correlator. Thus, the  $\alpha$ -peak strengths, widths, and positions are correlated. These correlations follow the same pattern as found and explained for the  $\alpha$  peaks of the hard-sphere system [13,14]. Nevertheless, it is not obvious from the beginning, and thus truly remarkable, that such a simple model will be sufficient not only to explain the trends found in the data, but even to reproduce structural relaxation for PC quantitatively.

Equation (3a) is equivalent to

$$\ddot{\phi}(t) + (\Delta + \nu)\dot{\phi}(t) + (\Omega^2 + \Delta \cdot \nu)\phi(t) + \Omega^2 \int_0^t m(t-t') [\dot{\phi}(t') + \Delta \cdot \phi(t')] dt' = 0, \quad (6)$$

to be solved with the initial condition  $\phi(t=0) = 1$ ,  $\dot{\phi}(t=0) = -\Delta$ . This equation, together with Eq. (3b), is solved numerically with a similar algorithm as used in the preceding work for the case  $\Delta = 0$ . Equations (5) are treated in the same manner, but  $\phi(t)$  has to be used as input for Eq. (5b). From the result for  $\phi_A^s(t)$ , a Laplace-transformation yields  $\phi_A^s(z)$ . The fluctuation-dissipation theorem then determines the dynamical susceptibility  $\chi_A(z)$  of variable  $A$ :

$$\chi_A(z)/\chi_A = z\phi_A^s(z) + 1. \quad (7)$$

Here,  $\chi_A \propto \langle A^2 \rangle$  is the thermodynamic susceptibility. In particular, the imaginary part of Eq. (7) determines the normalized susceptibility spectrum,  $\chi_A''(\omega)/\chi_A = \omega\phi_A^s''(\omega)$ , the

quantity of main interest in the following. In our data analysis,  $\chi_A$  enters as an additional fit parameter, which we treat, for the sake of simplicity, as a temperature-independent normalization constant.

### III. DATA ANALYSIS

#### A. Fits to the data

The result of our fits to the measured PC spectra are shown by the full lines in Figs. 1 and 2. Since one cannot expect the schematic model to provide a description of the microscopic band, the fits have been restricted to frequencies below 500 GHz for the light-scattering and neutron-scattering spectra. The fit range for the dielectric spectra could be extended up to 1 THz. For the neutron-scattering data, a set of spectra for 3 representative  $q$ -vectors out of 10 analyzed is shown. The analyzed  $q$ -range is  $0.5 \text{ \AA}^{-1} \leq q \leq 1.4 \text{ \AA}^{-1}$ ; outside this range, experimentally accessible frequency windows become too small to gain meaningful information for MCT parameters. In Ref. [1], light-scattering spectra above  $T = 250$  K have been published, but show apparent violation of  $\alpha$  scaling. We were able to fit these curves with the same quality as the ones shown by assuming a slightly varying static susceptibility  $\chi_{ls}$ , which has the effect of shifting curves up and down in the log-log plot. These curves were omitted in Fig. 1 to avoid overcrowding.

All model parameters should be used as temperature-dependent fit parameters in our analysis. Within the studied temperature interval, there are no structural anomalies reported for PC. Thus, the fits are done with the constraint that the parameters drift smoothly and monotonously. In the following part of this section, the parameters used for the theoretical curves in Figs. 1 and 2 shall be discussed.

One experiences a considerable flexibility in choosing the path  $(v_1(T), v_2(T))$  followed by the coupling constants in the  $v_1$ - $v_2$ -parameter plane for the interpretation of the data as emphasized earlier [24]. To arrive at an overview of the possibilities for fitting the many

spectra, we started with a first step, where the path was varied but biased to some smooth curve. Applying the general theory [27] to Eq. (3b), one derives the formula for the above-mentioned separation parameter  $\sigma$ ,

$$\sigma = (1 - f^c) \left[ (v_1 - v_1^c) f^c + (v_2 - v_2^c) f^{c2} \right]. \quad (8)$$

In our first step of the analysis, we also force the  $v_1, v_2$  to obey the asymptotic linear  $(T_c - T)$  dependence of  $\sigma$  cited above. In the second step, this latter restriction is eliminated and a free fit is started by examining small corrections to the result of the first step. The thus obtained results also account for an inevitable uncertainty in the determination of the experimental temperatures. The fit yields  $T_c \approx 180$  K, and  $\lambda \approx 0.75$ , corresponding to  $a \approx 0.30$  and  $b \approx 0.56$ . The value for  $\lambda$  is between the values reported in Refs. [1] and [10] and falls within the error bars of both. The linear interpolation of the found  $\sigma$  versus  $T$  values gives  $\sigma = C(T_c - T)/T_c$  with  $C \approx 0.069$ . The found distribution of  $(v_1, v_2)$  points is shown in the upper part of Fig. 3. Upon lowering  $T$ , both  $v_1$  and  $v_2$  increase, which is consistent with the physical reasoning of the system's mode-coupling coefficients becoming larger at lower temperatures. The lower diagram in Fig. 3 demonstrates that the asymptotic formula for  $\sigma$  is well obeyed for  $150$  K  $\leq T \leq 285$  K. It should be stressed that the glass-transition line is just crossed by a regular drift, i. e. there is no accumulation of  $(v_1, v_2)$  points close to it. This demonstrates how the critical phenomena predicted by the MCT originate from the mathematical structure of its equations of motion. In particular, the schematic model illustrates that within MCT no subtle  $q$ -interferences or hydrodynamic phenomena are responsible for the glass-transition dynamics.

The fitted mode-coupling coefficients  $v_A^s(T)$  for the light-scattering and dielectric data, and the corresponding coefficients  $v_{\text{ns}}^s(q, T)$  for the neutron-scattering experiment are shown in Fig. 4. Again, we find monotonically increasing couplings with decreasing temperature. The coupling coefficients  $v_{\text{ns}}^s(q)$  describing the incoherent-neutron-scattering data are decreasing with increasing  $q$ . This is equivalent to the plateau values  $f_q^{s,c}$  decreasing with increasing  $q$ , which agrees qualitatively with the findings for incoherent-neutron-scattering

results discussed within the microscopic MCT [14].

The parameters  $\Omega_A^s$ ,  $\nu_A^s$  which specify the transient dynamics of  $\phi_A^s$  are shown in Fig. 5. The results from the neutron-scattering analysis reflect the behavior  $\Omega_{\text{ns}}^s(q, T) \propto q \cdot \sqrt{T}$  to a good approximation, which is in agreement with the result of the microscopic theory. But drawing more conclusions from the microscopic parameters would be over-interpreting the model. They are shown here mainly to demonstrate that there are no abnormal variations occurring. We find much larger uncertainties for the microscopic fit parameters  $\Omega$ ,  $\nu$ ,  $\Omega_A^s$ ,  $\nu_A^s$ , than for those parameters  $v_1$ ,  $v_2$ , and  $v_A^s$ , ruling the structural-relaxation part of the spectra. In particular, it was possible to use for the parameters which specify the transient of the first correlator  $\phi(t)$  temperature independent values  $\Omega = 1 \text{ THz}$  and  $\nu = 0 \text{ THz}$ .

The hopping coefficient  $\Delta$  in Eq. (3a) determines the position of the susceptibility minimum below  $T_c$ . This minimum cannot be seen in the light-scattering data, thus the chosen values are not unambiguously determined. The light-scattering spectra in the upper panel of Fig. 1 are fitted with the hopping parameter  $\Delta_A^s$  for the second correlator ignored:  $\Delta_{\text{ls}}^s = 0$ . The fits to the dielectric-loss spectra in the lower panel of Fig. 1 are done with a non-vanishing  $\Delta_{\text{de}}^s$ . For the whole temperature range investigated,  $\Delta(T)$  can be assumed to follow an Arrhenius law,  $\Delta(T) \propto \exp(-E_A/T)$ , which would be expected for thermally activated hopping over barriers. Fig. 6 shows the values used for the fit. Although  $\Delta$  increases by an order of magnitude, the calculated curves for temperatures higher than 190 K show no influence from hopping effects on the spectra. This is demonstrated in Fig. 7. The irrelevance of the increasing hopping coefficients  $\Delta_q$  for temperatures increasing above  $T_c$  can be understood on the basis of a discussion of the asymptotic formulas [28]. It is the reason, why the idealized theory can be used for data analysis for  $T$  sufficiently larger than  $T_c$ . In the analyzed neutron-scattering experiment, the dynamical window and the studied temperature intervals are too small to investigate hopping effects, and therefore the curves in Fig. 2 are calculated with  $\Delta_{\text{ns}}^s = 0$ .

Above  $T_c$ , the spectra including hopping show deviations from the idealized ones only for small  $T - T_c$ . Below  $T_c$ , the crossover to the white-noise spectrum is suppressed, and

a minimum occurs as hopping starts to be the dominant relaxation effect. Because of the insensitivity of the main body of the analyzed data to choices of  $\Delta$ , the activation energy cannot be determined very precisely from the fit; the upper straight line in Fig. 6 corresponds to  $E_A = 811$  K. This value is in reasonable agreement with the one found in an earlier asymptotic analysis [1]. Dielectric-loss spectra show hopping-induced minima at higher frequencies than the light-scattering spectra, and this we have accounted for by introducing a second hopping parameter  $\Delta_{\text{de}}^s$  there. In a similar way,  $(\Omega_{\text{de}}^s/\Omega)^2 \Delta_{\text{de}}^s(T)$  follows an Arrhenius law and has no influence on the spectra above  $T_c$ ; this second hopping term has already been included in the comparison studied in Fig. 7. Here, the activation energy is of the order of 2000 K, which makes the result more striking, since  $(\Omega_{\text{de}}^s/\Omega)^2 \Delta_{\text{de}}^s$  is allowed to vary over three orders of magnitude. In both cases, activation energies as well as the prefactors are of reasonable magnitude. It should be stressed that, although the treatment of hopping by a frequency-independent  $\Delta$  is rather crude, the resulting frequency range in which the schematic model gives a good fit to experimental data, is enlarged by about one decade for  $T < T_c$  relative to the fit interval which can be treated by the idealized-MCT model.

In the measurements of the dielectric functions, information on both the imaginary and the real part of  $\varepsilon(\omega) = \varepsilon'(\omega) + i\varepsilon''(\omega)$  have been obtained [6]. The fit to the  $\varepsilon''$  data shown above was performed using  $\varepsilon''(\omega) = 4\pi\chi_{\text{de}}''(\omega) = 4\pi\chi_{\text{de}}\omega\phi_{\text{de}}^s''(\omega)$ , thus obtaining the proportionality factor  $\varepsilon_0 = 4\pi\chi_{\text{de}}$  as a by-product. Then, the real part is given by  $\varepsilon'(\omega) - \hat{\varepsilon} = \varepsilon_0 \cdot (1 + \omega\phi_{\text{de}}^s(\omega))$ . The new parameter  $\hat{\varepsilon}$  has to be determined by shifting the curves, and it can differ from  $\varepsilon_\infty = 1$  in both directions: The liquid exhibits microscopic oscillations, which contribute to  $\varepsilon'(\omega)$  as some shift  $\Delta\varepsilon_{\text{micr.}}^{\text{exp.}}$  with respect to  $\varepsilon_\infty = 1$  for the structural part of the response function. The schematic model uses a single damped oscillator, giving some  $\Delta\varepsilon_{\text{micr.}}^{\text{fit.}}$ , which may be either too small or too large. Depending on the temperature, we find values of  $\hat{\varepsilon} = \varepsilon_\infty + (\Delta\varepsilon_{\text{micr.}}^{\text{exp.}} - \Delta\varepsilon_{\text{micr.}}^{\text{fit.}})$  between 3 and -1, which are of reasonable magnitude. Figure 8 shows the result of testing our fit against the accordingly shifted real part of the measured dielectric function. It is clear from the theory that the real and

imaginary parts of the calculated curves are connected by Kramers-Kronig relations. But for the experiment, both quantities have to be regarded as almost independent data sets, since the measurements are restricted to a finite frequency range. Thus, figure 8 provides more than just a different view on the fit shown in Fig. 1, and it is an important point that the real-part data can be fitted with the schematic model as well, introducing only one additional fit parameter  $\hat{\varepsilon}$ . In the minimum region of the spectra, we find this to be confirmed, and for higher  $T$ , the  $\alpha$ -relaxation step can be described by the schematic model, too. The discrepancies for the  $\alpha$  peak in the glass are the analogue to what can be seen in the  $\varepsilon''$  fit. Similar observations hold for the high-frequency dynamics, where one has to notice in addition, that experimental error bars are relatively large for frequencies above 300 GHz. A slightly better fit of the  $\varepsilon'$  data could have been achieved by allowing the static susceptibility  $\chi_{\text{de}}$  to vary with temperature. This possibility is not examined here, since the shift is only small, and since we do not want to introduce assumptions on the  $T$ -dependence of the static quantity  $\varepsilon_0$ .

## B. Summary of the Data Analysis

Glass-forming liquids exhibit temperature-sensitive spectra for frequencies well below the band of microscopic excitations. These precursors of the glass transition are referred to as structural-relaxation spectra. The full lines in Fig. 1 and 2 demonstrate, that the evolution of structural relaxation of PC, including the crossover to the microscopic regime, is described well by a schematic MCT model. The description holds for all spectra obtained by the depolarized-light-scattering spectrometer; in this case it deals with the three-decade dynamical window between 0.3 and 500 GHz, and it accounts for the change of the spectral intensity by a factor of  $10^3$  if the temperature is shifted between the glass transition  $T_g$  and 30 K above the melting temperature  $T_m$ . It accounts for the measured  $\alpha$ -peak-maximum shift by a factor of 10 if  $T$  is changed by 30 K. A similar statement holds for the description of the dielectric-loss spectra, where the  $\alpha$ -peak shift from 40 GHz down to 0.02 GHz is described.

This shift is caused by a temperature decrease from  $293\text{ K} = T_m + 75\text{ K}$  to  $243\text{ K}$ .

Between the  $\alpha$  peak and the vibrational excitation peak near  $1\text{ THz}$ , the susceptibility spectra in Figs. 1 and 2 exhibit a minimum at some frequency  $\omega_{\min}$ . It shifts to smaller frequencies as the temperature is lowered, but less than the  $\alpha$ -peak position. Its intensity  $\chi_{\min} = \chi''(\omega_{\min})$  exceeds the white-noise spectrum one would expect for the dynamics of normal liquids by more than two orders of magnitude. Such white noise would yield susceptibility spectra varying linearly with frequency,  $\chi''_{\text{wh.n.}}(\omega) \propto \omega$ , as is indicated by the dashed lines in Fig. 1. These anomalous minima are also treated properly by the model.

Neutron-scattering data are available for a series of wave vectors  $q$ , and hence the dynamics is probed on various length scales. The  $q$  dependence is in the schematic model described by that of the coupling coefficient  $v_{\text{ns}}^s(q)$ . The data description in Fig. 2 is possible using a  $q$  dependence in qualitative agreement with the results expected from the microscopic theory of simple systems.

It appears nontrivial that the used schematic model can deal with the mentioned spectra of PC. The success of the fits indicates that the studied glassy dynamics is rather insensitive to microscopic details of the systems. Apparently the evolution of glassy dynamics within the GHz window reflects, above all, only quite general features of the nonlinear-interaction effects, which can also be modelled by simple truncations of the full microscopic theory. These conclusions require some reservation. The explanation of the PC data by the used model is based on the choice of the model parameters, in particular on the choice of the drift of all parameters with changes of temperature, which is documented in Fig. 3-6. Only a full microscopic theory can show, whether or not the chosen parameters are in accord with the fundamental microscopic laws.

Furthermore, it has to be emphasized that the studied model cannot reproduce the spectra for frequencies below  $1\text{ GHz}$  if the temperature is below the critical value  $T_c$ . Such spectra can be measured accurately using dielectric-loss spectroscopy, and the lower panel of Fig. 1 exhibits some of this data for  $T = 173\text{ K}$  and  $T = 183\text{ K}$ . The lack of success of our work in handling these spectra is clearly connected with the improper treatment

of hopping processes. It remains unclear at present, whether this is due to the stochastic approximation,  $N_q(z) = i\Delta_q$ , or due to restricting ourselves to a one-component schematic model, or whether the whole extension of MCT to a theory including hopping transport is inadequate.

#### IV. SOME ASYMPTOTIC FORMULAS

Let us list some of the asymptotic results for the studied MCT model, which will be needed below in Sec. V. These results are obtained by straight-forward specialization of the general formulas discussed in Ref. [27]. We will focus on the  $\beta$ -relaxation regime for  $T \geq T_c$ , with hopping effects neglected. A comprehensive discussion of the asymptotic results can be found in Ref. [13].

From the full MCT equations (1), a leading-order expansion in  $\sqrt{|\sigma|}$  gives rise to the asymptotic predictions for the intermediate-time window of the  $\beta$  relaxation. A central result is the factorization theorem,  $\phi_q(t) - f_q^c = h_q G(t)$ , where the so-called  $\beta$  correlator  $G(t)$  is independent of  $q$ . This result still holds, in the generic case, for the tagged-particle density-fluctuation correlator or the correlator dealing with light scattering or dielectric response:  $\phi_A^s(t) = f_A^{s,c} + h_A^s G(t)$ , with the same  $G(t)$  as above. The Fourier-cosine transform of  $G(t)$  is called the  $\beta$  spectrum  $G''(\omega)$ . One gets for the normalized susceptibility spectra

$$\chi''_x(\omega) = \omega \phi''_x(\omega) = h_x \chi''(\omega) , \quad (9)$$

where  $\chi''(\omega) = \omega G''(\omega)$  is called the  $\beta$ -susceptibility spectrum. Here, the index  $x$  denotes either the wave-vector modulus  $q$ , or  $x = (s, A)$ . The function  $G$  depends on  $t/t_0$ ,  $\sigma$ , and  $\delta$  only: it is uniquely determined by the exponent parameter  $\lambda$  as the solution of the equation

$$\sigma - \delta t + \lambda(G(t))^2 = \frac{d}{dt} \int_0^t G(t-t')G(t') dt' , \quad (10)$$

to be solved with the initial condition  $G(t \rightarrow 0) = (t/t_0)^{-a}$ . The so-called hopping parameter  $\delta$  has to be calculated from  $\Delta_q$ , and for the studied model it reads

$$\delta = \Delta f^{c2} / (1 - f^c) . \quad (11)$$

In this context, the numbers  $\Delta_A^s$  only enter as corrections to scaling.

The plateau values  $f_x^c$ , and the critical amplitudes  $h_x$  can be calculated from the mode-coupling functionals. In the case of the schematic model studied, the values for the first correlator are given by  $\lambda$ :

$$f^c = 1 - \lambda, \quad h = (1 - f^c) . \quad (12)$$

The relation between the exponent parameter  $\lambda$  and the  $\alpha$ -peak strength  $f^c$  is one of the non-generic features of that model. For the second correlator, the plateau value and critical amplitude read

$$f_A^{s,c} = 1 - \frac{1}{v_A^s f^c}, \quad h_A^s = \frac{1 - f^c}{v_A^s f^{c2}} . \quad (13)$$

Changing  $v_A^s$ , the  $\alpha$ -peak strength  $f_A^{s,c}$  can be varied. Again, these equations establish a non-generic relation between the  $f_A^{s,c}$  and the  $h_A^s$ . In our fits to the neutron-scattering data, a  $q$  dependence of  $f_{\text{ns}}^{s,c}$  and  $h_{\text{ns}}^s$  can arise only through a  $q$ -dependence of the  $v_{\text{ns}}^s$ .

From Eq. (10) one identifies for the case  $\delta = 0$  the time scale for the  $\beta$ -relaxation:  $t_\sigma = t_0 |\sigma|^{-1/2a}$ . Going over to rescaled times,  $\hat{t} = t/t_\sigma$ , and rescaled frequencies,  $\hat{\omega} = \omega t_\sigma$ , one gets from Eq. (9) the scaling law for the  $\beta$ -susceptibility spectra

$$\chi''_x(\omega) = h_x c_\sigma \hat{\chi}(\hat{\omega}) , \quad (14)$$

where  $c_\sigma = \sqrt{|\sigma|}$ . The master spectrum  $\hat{\chi}$  is  $\sigma$ -independent. It is fixed through the exponent parameter  $\lambda$ , and thus through the static structure alone. For large rescaled frequencies,  $\hat{\omega} \gg 1$ , one obtains the critical-power-law spectrum. This extends to all frequencies as  $\sigma \rightarrow 0$ :

$$\chi''_x(\omega) = h_x \cdot \sin(\pi a/2) \Gamma(1 - a) (\omega t_0)^a, \quad T = T_c . \quad (15)$$

For small rescaled frequencies, one gets the von Schweidler-law for  $\sigma < 0$ ,  $\hat{\chi}(\hat{\omega} \ll 1) \propto 1/\hat{\omega}^b$ , and thus  $\hat{\chi}$  exhibits a minimum at some frequency  $\hat{\omega}_{\text{min}}$  with  $\hat{\chi}_{\text{min}} = \hat{\chi}(\hat{\omega}_{\text{min}})$ . Due to

the scaling law, Eq. (14), the variation of the spectral minima with temperature is, in the asymptotic region, given by

$$\omega_{\min} = \hat{\omega}_{\min}/t_\sigma, \quad \chi_{\min} = \hat{\chi}_{\min} \cdot c_\sigma, \quad \sigma < 0. \quad (16)$$

The point  $(\hat{\omega}_{\min}, \hat{\chi}_{\min})$  is completely fixed by  $\lambda$ , and for  $\lambda = 0.75$  one gets:  $\hat{\omega}_{\min} = 1.733$ ,  $\hat{\chi}_{\min} = 1.221$ .

On the glass side,  $\sigma > 0$ , the idealized theory yields for the  $\beta$  correlator for large rescaled times a constant,  $G(\hat{t} \gg 1) = 1/\sqrt{1 - \lambda}$ . Thus the signature of the MCT-fold bifurcation are  $\sqrt{T_c - T}$  anomalies of the nonergodicity parameters  $f_x = \phi_x(t \rightarrow \infty)$ :

$$f_x(T) = f_x^c + h_x \sqrt{\sigma/(1 - \lambda)}, \quad T < T_c. \quad (17)$$

If the correlators deal with density fluctuations or tagged-particle densities, the quantity  $f_x$  is the Debye-Waller factor or Lamb-Mößbauer factor, respectively. For  $\sigma < 0$ , corresponding to  $T > T_c$ , the long-time limits of the correlators vanish, as is the case for  $T < T_c$  but  $\delta \neq 0$ . But if  $\sigma$  and  $\delta$  are sufficiently small, the correlators still exhibit plateaus for times exceeding the transient scale  $t_0$  before the decay towards zero sets in. The heights of these plateaus are then given by  $f_x$  for  $T < T_c$ , and by  $f_x^c$  for  $T > T_c$ , then called effective nonergodicity parameters. The decay from the plateau is the  $\alpha$  process, and thus the strength of the  $\alpha$  peak in the susceptibility spectra is given by  $f_x$ . This also corresponds to the height of the relaxation step exhibited by the real part of the susceptibility, when the frequency is shifted through the  $\alpha$ -peak window.

The preceding Eqs. (9-17) establish universality features of MCT. They provide the basis of a general explanation of the glassy MCT dynamics by means of features of the spectra not depending on the specific microscopic properties of a given system.

## V. SCALING LAW ANALYSIS

In this section it shall be studied how well the above calculated MCT solutions can be described by the MCT- $\beta$ -relaxation-scaling laws summarized in the preceding section. It has

been demonstrated earlier [13,14], that the range of validity of these equations can be analyzed by evaluating the next-to-leading-order corrections. Here, we will study the combined effect of all corrections due to structural relaxation as well as due to vibrational-transient-dynamics effects. Only the solutions referring to the parameter sets used in Figs. 1 and 2 will be discussed. Thus the following analysis refers to control parameters and dynamical windows representative for state-of-the-art experimental studies of the evolution of glassy dynamics.

### A. The critical decay

Solving the equations of motion for  $T = T_c$ ,  $\Delta = 0$ , and  $\Delta^s = 0$  for times up to  $10^{15}$  ps, the critical power law, Eq. (2), was identified. The common time scale was determined to  $t_0 = 0.035$  ps. The leading-order result  $\hat{\phi}_x(t) = (t/t_0)^{-a}$ , where  $\hat{\phi}_x(t) = (\phi_x(t) - f_x^c)/h_x$ , is shown in the double-logarithmic representation of Fig. 9 by straight dash-dotted lines with slope  $-a$ . For the two temperatures closest to  $T_c$ , the full lines in this diagram exhibit the solutions  $\hat{\phi}_x(t)$ . Dashed lines demonstrate the corresponding  $\beta$  correlators  $G(t)$ , determined from Eqs. (8,10,11). The approach of the first correlator  $\phi(t)$  towards the plateau  $f^c$  is well described by the scaling law for  $T = 180$  K and  $190$  K. For  $T = 180$  K the critical power law is exhibited within a 1.5-decade time window for times exceeding  $t_c$  with  $t_c/t_0 \approx 300$ , while for  $t < t_c$  the vibrational transient dynamics masks the structural relaxation. In this case, the validity of the critical power law for larger times is restricted by the onset of hopping effects. Hopping plays no significant role for the  $\beta$  relaxation of  $T = 190$  K (compare Fig. 7). But there, the deviations of  $G(t)$  from the short-time limit  $(t/t_0)^{-a}$  set in already for  $t < t_c$ . Thus this power law cannot be identified anymore for distance parameters  $\varepsilon = (T_c - T)/T_c$  with  $|\varepsilon| \gtrsim 0.06$ . This scenario is in semiquantitative agreement with the one discussed in Ref. [29] for the density correlators of a hard-sphere system. Let us reiterate that the correlator  $\phi(t)$  drives the glass transition for the studied model, but that it is not the quantity measured. The two lower sets of curves in Fig. 9 show that the decrease of  $\phi_{ls}^s(t)$  and  $\phi_{de}^s(t)$  towards

their plateaus  $f_{ls}^{s,c}$  and  $f_{de}^{s,c}$  respectively is described qualitatively by the dashed lines, i. e. by the scaling laws. However, there are remarkable quantitative deviations between the solutions  $\hat{\phi}_A^s(t)$  and their asymptotic form  $G(t)$ . These appear as if the amplitude experiences some offset. The reason is that the transient dynamics influences the correlators  $\phi_A^s(t)$  also for times which exceed  $t_c$  by up to two orders of magnitude. This means that the dynamics of the two probing variables is strongly influenced by oscillations within that window, where the driving correlator  $\phi(t)$  exhibits the  $t^{-a}$  law. Therefore the power law  $\hat{\phi}_A^s(t) = (t/t_0)^{-a}$  cannot be identified accurately in the curves shown for  $A = ls$  and  $A = de$ . This is also demonstrated by the straight dash-dotted line in the upper panel of Fig. 1, which represents the asymptotic low-frequency-susceptibility spectrum at the critical point, Eq. (15).

Within the 1.5-decade window, where the  $\log \hat{\phi}$ -versus- $\log(t/t_0)$  curve for 180 K in Fig. 9 demonstrates the critical-decay asymptote, the graphs of  $\log \hat{\phi}_{ls}^s$  and  $\log \hat{\phi}_{de}^s$  versus  $\log(t/t_0)$  for 180 K and 183 K, respectively, also appear as nearly straight lines, so that they can be described very well in this window by some effective power law. One thus expects an effective power-law spectrum which is described by Eq. (15), but with  $a$  and  $h_A$  replaced by some  $a^{\text{eff}}$  and  $h_A^{\text{eff}}$  respectively. This phenomenon also was observed for the susceptibility spectra of the hard-sphere system [29]. For the light-scattering result, one infers  $a^{\text{eff}} < a$  and  $h_{ls}^{\text{eff}} < h_{ls}^s$ . The dotted line in the upper panel of Fig. 1 corroborates this conclusion. It exhibits the solution for the model evaluated for  $T = T_c$  with hopping effects ignored. This line can be fitted well between  $10^{-5}$  THz and  $10^{-3}$  THz by an effective power-law following Eq. (15) with  $a^{\text{eff}}/a \approx 0.92$  and  $h^{\text{eff}}/h \approx 0.7$ . The crossover from this effective power law to the asymptotic critical law, Eq. (15), occurs only at frequencies around 1 MHz.

## B. The non-ergodicity-parameter anomaly

Figure 10 shows effective nonergodicity parameters of the three correlators underlying the curves in Fig. 1, which were determined from the plateau heights of the  $\phi_x(t)$ -versus- $\log t$  diagrams. The crosses in the lower panel show the values deduced in Ref. [6] from

the step size of the measured real part of the dielectric function, divided by the value of  $\varepsilon_0$  assumed in the fit to the susceptibility spectra. Figs. 1 and 8 demonstrate that the present model describes the dielectric function of PC reasonably, and so it is not surprising that the calculated values (dots) reproduce the measured ones (crosses) reasonably well. The discrepancies between dots and crosses are anticipated to be mainly due to difficulties in determining the step size accurately in the experiment, where one carefully has to eliminate contributions from the  $\beta$  relaxation.

Full lines in Fig. 10 exhibit the asymptotic laws, i. e. the values  $f_x$  from Eq. (17) for  $T < T_c$  and the constant  $f_x^c$  for  $T \geq T_c$ . Figure 10(a) demonstrates that the 60% variation of the effective non-ergodicity parameter  $f$  of the first correlator is described well by the asymptotic formula. This holds for temperatures down to  $T_g$ . On the other hand, the results for the light scattering and for the dielectric response do not exhibit the asymptotic behavior; there is no evidence for the  $\sqrt{T_c - T}$  anomaly at all to be noticed in the data. There are two reasons for this finding. The obvious one reflects the large size of  $f_A^{s,c}$ , i. e. it results from the observation that the  $\alpha$  peaks of the susceptibility dominate over the remaining susceptibility spectrum (compare Fig. 1). Equation (17) for probing-variable correlator is equivalent to

$$(1 - f_A^s) = (1 - f_A^{s,c}) - h_A^s \sqrt{\sigma/(1 - \lambda)} . \quad (18a)$$

Since  $(1 - f_A^s)$  and  $h_A^s$  are positive and  $(1 - f_A^{s,c})$  is less than 0.1 for the two correlators discussed, the whole  $\sqrt{T_c - T}$  effect is below 10%. Therefore it is difficult to separate the  $\sqrt{T_c - T}$  anomaly from the scatter of the data. The less obvious reason results from the smooth but appreciable temperature drift found for the coupling coefficient  $v_A^s$  (compare Fig. 4). This coupling determines the non-ergodicity parameters of the second correlator of the schematic model in terms of the parameter  $f$ :  $(1 - f_A^s) = 1/(v_A^s f)$ . The square-root singularity is due to that in  $f$ , and expanding  $(1/f)$  one reproduces Eq. (18a), but with effective terms

$$(1 - f_A^{s,c})^{\text{eff}} = R_A(1 - f_A^{s,c}), \quad h_A^{\text{eff}} = R_A h_A^s,$$

$$R_A(T) = v_A^{s,c}/v_A^s(T) . \quad (18b)$$

Replacing the renormalization coefficient  $R_A(T)$  by its value at the critical point,  $R_A^c = 1$ , one reproduces the leading-order result, Eq. (17). However, within the temperature interval considered, the smooth drift of  $(1 - f_A^{s,c})^{\text{eff}}$  overwhelms the small variation of the  $\sqrt{T_c - T}$  term. This is demonstrated in Figs. 10(b,c) by the dashed lines. The numerically found circles are well described by this line. One concludes that the drifting coupling coefficient  $v_A^s(T)$  is responsible for the deviations from the leading-order asymptotics. Unfortunately, the  $v_A^s(T)$  are not available directly from experiments.

### C. Scaling of the $\beta$ -relaxation minima

Figure 11 shows the susceptibility master spectrum  $\hat{\chi}$  for  $\lambda = 0.75$  and  $\delta = 0$  as dashed curves. The upper set of solid lines in this figure are the spectra of the first correlator rescaled, according to Eq. (14), as  $\omega\phi''(\omega)/(\sqrt{|\sigma|}h)$ . Asymptotic validity of scaling is demonstrated: the window of rescaled frequencies  $\hat{\omega} = \omega t_\sigma$ , for which the rescaled spectra are close to the master spectrum  $\hat{\chi}$ , expands with decreasing  $(T - T_c)$ . Convincing agreement between  $\hat{\chi}$  and the 180 K result can be found as long as hopping effects are ignored. For higher temperatures, where  $|\varepsilon| = |T - T_c|/T_c \geq 0.06$ , strong deviations are found. The  $T = 210$  K spectrum, for which  $|\varepsilon| = 0.17$ , does not even show a minimum. The demonstrated deviations from the scaling laws are similar to what was explained in Ref. [13] for the MCT solutions for the hard-sphere system.

Preasymptotic-correction effects for the variables discussed for PC in Figs. 1 and 2 differ from those for the auxiliary correlator  $\phi$ . This is demonstrated in the lower part of Fig. 11 for  $\varepsilon = -0.17$ . Deviations of the rescaled spectra  $\chi_A''(\omega)/(\sqrt{\sigma}h_A)$  from the master spectrum  $\hat{\chi}(\omega t_\sigma)$  are larger for the dielectric loss than for the light scattering, and the latter are larger than those for the neutron-scattering results. While the predicted probe independence of  $\chi_A''(\omega)/h_A$  holds rather well for  $\omega < \omega_{\min}$ , deviations from the factorization theorem are observed mainly for higher frequencies. As discussed above in connection with Eq. (18a),

the large size of  $f_A^{s,c}$  leaves only a 10% decay of the correlator from the initial value unity to the plateau, and this decay is influenced by vibrational motion. This leads to the strong disturbances of the susceptibility spectra for  $\omega > \omega_{\min}$ . For the neutron-scattering data for intermediate wave vectors, this problem is not so severe, since the critical Lamb-Mößbauer factor  $f_q^c$  decreases with increasing  $q$ . Therefore the shape of the susceptibility minimum, which is exhibited by the two neutron-scattering results shown in Fig. 11, is closer to the one of the master spectrum.

The  $q$ -dependence of the critical amplitude  $h_q^s$  for the incoherent-neutron-scattering spectra has been measured as a byproduct of the test of the factorization theorem,  $\phi_q^{s''}(\omega) \propto h_q^s \chi''(\omega)/\omega$ . A linear law,  $h_q^s \propto q$ , was found within the studied wave-vector interval [10]. Such a strictly linear law is not compatible with the microscopic MCT, which predicts that the  $h_q$ -versus- $q$  graph exhibits a broad asymmetric peak near the position  $q_{\max}$  of the first sharp diffraction peak of the structure factor. For small  $q$ , the critical amplitude increases regularly as  $h_q \propto q^2 + \mathcal{O}(q^4)$  [14], and thus  $h_q$  exhibits an inflection point for some  $q < q_{\max}$ . Whether the found linear  $q$ -dependence of the experimental values is due to multiple-scattering effects, is not clear [10]. Our schematic-model fit, however, suggests that, even if  $h_q^s$  can be approximated by a linear law, the  $q$ -dependence is not strictly linear but rather given by some intermediate crossover around the inflection point. Equation (13) relates  $h_q^s$  to the inverse of  $v_q^s$ ; thus a strictly linear law for  $h_q^s$  would imply  $v_q^s \propto 1/q$ . Such result is added as a dash-dotted line in Fig. 4b, and it shows that this is not consistent with our data analysis. An ad-hoc expression, reflecting the crossover from the small- $q$  asymptote through the inflection point is  $h_q^s \propto q^2 / [1 + (q/q^*)]$ . The resulting expression for  $v_q^s$  is added in Fig. 4b as dashed lines for two temperatures, and it provides a reasonable interpolation of the found fit parameters. One would need measurements for wave vectors of the order of  $0.2 \text{ \AA}^{-1}$  and less, in order to test for the small- $q^2$  behavior predicted by the microscopic MCT.

There is a most bothersome preasymptotic-correction effect which can be seen in the lower part of Fig. 11: the positions  $\omega_{\min} t_\sigma$  of the susceptibility minima are not identical;

and they are all larger than the asymptotic value  $\hat{\omega}_{\min}$  which is shown by a diamond. Since the bands of microscopic excitations of the correlator spectra  $\phi_A''(\omega)$  are located at much lower frequencies than that of the spectrum  $\phi''(\omega)$ , the spectrum of the test variables cross over too quickly to the transient to be able to develop the universal relaxation pattern for  $\omega > \omega_{\min}$ . As a result,  $\omega_{\min}$  gets an offset to larger frequencies. Figure 12 exhibits this result as a rectification diagram. The asymptotic result is shown as a full straight line:  $\omega_{\min}^{2a} = (\hat{\omega}_{\min}/t_0)^{2a} |\sigma| = \hat{C}(T - T_c)$  with the constant  $\hat{C} = (\hat{\omega}_{\min}/t_0)^{2a} \cdot C/T_c \approx 0.004$ . The positions of the observed minima can still be interpolated reasonably by straight lines, shown in dashed. However, the slopes of the dashed lines differ from those of the asymptotic line. In a clear violation of the asymptotic factorization theorem, the lines for different probing variables are different. The linear interpolations lead to intersections with the abscissa, which differ somewhat from the correct value of  $T_c$ . For the neutron-scattering data, this interpolation has been omitted in Fig. 12, since the error bars obtained by  $q$ -averaging do not allow for a well-determined estimate here.

There is also a strong temperature-dependent offset of the amplitude scale relative to the scaling-law prediction. This is demonstrated in Fig. 13 for the light-scattering spectra. All four rescaled minima  $\chi_{\min}/\sqrt{\sigma}h_{ls}$  are far below  $\hat{\chi}_{\min}$ , which is indicated by a diamond. Moreover, with decreasing  $(T - T_c)$ , the discrepancy between rescaled curves and expected asymptote does not decrease, rather it increases. Such behavior is not anticipated from the leading-order corrections to the scaling laws [13,14], but it can be explained as a higher-order effects because of the important role played by the temperature dependence of the coupling coefficient  $v_A^s$ . This drift can be eliminated by introducing an effective amplitude  $h_{ls}^{\text{eff}}$ , as discussed above in connection with Eq. (18b). The result is given by the upper set of curves in Fig. 13. Indeed, the discrepancies between asymptotics and rescaled curves are reduced, and they now decrease with decreasing  $(T - T_c)$ . But even for  $T = 190$  K, i. e. for  $|\varepsilon| = 0.06$ , there is a considerable offset of the minimum intensity from the scaling result. The 180 K curve demonstrates the approach towards the asymptotic limit, would hopping be absent. There still is a clear deviation between rescaled spectrum and scaling-law result,

which increases with increasing  $\omega$  for  $\omega > \omega_{\min}$ . But the sign and size of this effect are similar to what was found for the hard-sphere system for wave vectors yielding a plateau  $f_q^c$  as large as  $f_{\text{ls}}^c$  [13].

#### D. Summary of the Scaling-Law Analysis

It is, of course, more satisfactory to interpret data for glassy dynamics with the set of universal formulas provided by MCT for the asymptotic dynamics near a glass-transition singularity than to explain experimental findings within schematic models. The more probing variables  $A$  are taken into account, the more convincing such an analysis is, since the universal results also imply connections between spectra measured for different  $A$ . The preceding work on PC [1,4–6,10] exemplifies these statements. However, the data are influenced by preasymptotic effects, and one cannot judge the relevance of these correction effects, if one does not know the underlying microscopic MCT equations. Forcing data into the universal formulas can thus lead to self-contradicting results, as the preceding subsections have demonstrated. While the spectral shapes are rather robust and the rectification diagram for the scales appears correct and leads to a reasonable estimation of  $T_c$ , as shown by the dashed lines in Fig. 12, the prefactors for the asymptotic formulas extracted from the data can be quite wrong. This error cannot be noticed if one studies a single probing variable  $A$  only, but it appears as a violation of the factorization theorem if one compares spectra for different  $A$ . One concludes that the problems with the analysis discussed in Ref. [10] are neither due to inadequate application of MCT results nor due to failures of MCT. Rather they reflect the properties of MCT; more precisely, they exemplify the limitations for the application of asymptotic laws.

A general rule [13,14] for the test of the  $\beta$ -relaxation-scaling law is corroborated by the present analysis: if the nonergodicity parameter  $f_A^c$  is large, i. e. if the  $\alpha$ -peak strength is large compared to the strength of the microscopic-excitation peak of the susceptibility spectrum, the preasymptotic corrections are very important. This is especially true for the

discussed light-scattering and dielectric-loss spectra. Neutron-scattering spectroscopy has the advantage that  $f_q^c$  can be shifted by changing the wave vector  $q$ . Therefore, we found the scaling-law analysis to work best for the neutron-scattering data of Ref. [10]. It would be very informative to corroborate this finding by a measurement of the expected  $\sqrt{T_c - T}$  anomaly of the Debye-Waller or Lamb-Möbbauer factor.

## VI. THE DIELECTRIC MODULUS

Since the memory kernel  $m_q^s(t)$  in the mode-coupling approach is expressed as a polynomial of the density correlators, Eq. (1c), this quantity shows the same asymptotic scenario as the correlators themselves. From the factorization theorem for the correlators one concludes in leading order for the kernels:  $m_A^s(t) = f_{M,A}^{s,c} + h_{M,A}^s G(t)$ . Eqs. (5b,12,13) determine the plateau  $f_{M,A}^{s,c}$  and the critical amplitude  $h_{M,A}^s$  for the memory kernel of probing variable  $A$ :

$$\begin{aligned} f_{M,A}^{s,c} &= v_A^s f^c f_A^{s,c}, \\ h_{M,A}^s &= v_A^s (f^c h_A^s + f_A^{s,c} h) = v_A^s h. \end{aligned} \quad (19)$$

While in the above discussion  $f_A^{s,c}$  was found to be larger than 90%, such that the square-root singularity is suppressed to a below-10% effect, the situation for the memory kernel is different. The coupling coefficient  $v_A^s$  now plays the role of a normalization constant. If one introduces the normalized memory kernel in analogy to the normalized correlators  $\phi_x(t)$ ,  $\hat{m}_A^s(t) = m_A^s(t)/v_A^s$ , such that  $\hat{m}_A^s(t \rightarrow 0) = 1$ , one gets for the normalized plateau:

$$\hat{f}_{M,A}^{s,c} = f^c f_A^{s,c}. \quad (20)$$

In cases where  $f_A^{s,c}$  is close to unity, like in our analysis of the dielectric-loss and light-scattering data, one can approximate  $\hat{m}_A^s(t) \simeq f^c + hG(t)$ . This equals the asymptotic expression for the first correlator. Thus, we can expect  $\beta$  scaling for the memory kernel of the probe-variable  $A$  to work equally well as for the first correlator and thus better than for the corresponding probe-variable correlator. Let us examine this in detail for the memory

kernel of  $\phi_{\text{de}}^s$  underlying the fit to the dielectric-susceptibility spectra. For the light-scattering data, qualitatively the the same picture arises.

In the upper part of Fig. 14, three spectra of the memory kernels for the dielectric function, rescaled to  $-\omega m''_{\text{de}}(\omega)/\sqrt{|\sigma|}$ , are plotted as solid lines for three temperatures above  $T_c$ . The asymptotic  $\beta$ -susceptibility spectrum for  $\lambda = 0.75$  is again shown as a dashed line. While the picture shows some similarity to the situation found in the upper part of Fig. 13 for the light-scattering susceptibilities, the reason for the deviations from the scaling law are different. This can be inferred from the lower part of Fig. 14, where the same scaling is shown for the normalized memory functions. Here, the solid lines represent  $-\omega \hat{m}_{\text{de}}''(\omega)/\sqrt{|\sigma|}h$ . One notices, that the  $\alpha$ -peak strength is remarkably smaller than in the dielectric susceptibility, and comparable to that for the first correlator of the model. Similarly, we find the standard scenario for the approach of the rescaled spectra to the master curve. The deviations from the asymptotics are qualitatively the same as exhibited in the upper part of Fig. 11 for  $\omega\phi(\omega)$ . Thus one concludes: the deviations from scaling seen in the upper part of Fig. 14 are mainly due to the  $T$ -dependent normalization  $v_A^s$ , and not, as in the case discussed in connection with Fig. 13, due to microscopic crossover effects.

The question of normalization becomes even clearer for the effective non-ergodicity parameters. Figure 15(a) shows the unnormalized values  $f_{M,\text{de}}^s$  as open circles. The full line exhibits the asymptotic prediction  $f_{M,\text{de}}^s = f_{M,\text{de}}^{s,c} + h_{M,\text{de}}^s \sqrt{\sigma/(1-\lambda)}$  for  $T < T_c$  and  $f_{M,\text{de}}^s = f_{M,\text{de}}^{s,c}$  for  $T \geq T_c$ . Again, the drifting coupling coefficient  $v_{\text{de}}^s$  is responsible for masking the predicted square-root law. But, unlike in Fig. 10, this is only true for the unnormalized quantity. The normalized function  $\hat{f}_{M,\text{de}}^s$ , shown as filled circles in Fig. 15(b), exhibits good agreement with the asymptotic law. As for the values discussed for the tagged-particle density correlators, the drift of  $v_{\text{de}}^s$  still results in a temperature dependence of  $\hat{f}_{M,\text{de}}^s$  for  $T > T_c$ , but this drift is now reduced to a 10% effect. The asymptotic value of  $\hat{f}_{M,\text{de}}^{s,c}$  differs only about 5% from the one for the first correlator,  $f^c$ , which is shown as a dash-dotted line in Fig. 15(b). It is remarkable, that even for the unnormalized quantity the position of  $T_c$  can be estimated better than it could be done for the plateau values of the tagged-particle

density correlators. This can be done by noticing that the slope of a linear interpolation of the data changes when going over from  $T < T_c$  to  $T > T_c$ .

From the MCT equations (1) with the hopping kernel set to zero, one derives the expression for the dynamic susceptibility, Eq. (7), in terms of the memory kernel  $m_A^s(z)$ ,

$$\chi_A(z) = -\Omega_A^s{}^2 \chi_A / \left[ z^2 - \Omega_A^s{}^2 + z M_A^{\text{reg}}(z) + \Omega_A^s{}^2 z m_A^s(z) \right]. \quad (21)$$

Let us define a dynamical susceptibility  $\chi_{M,\text{de}}(z)$  corresponding to the kernel  $m_{\text{de}}^s(t)$  in analogy to Eq. (7):

$$\chi_{M,\text{de}}(z) = z m_{\text{de}}^s(z) + m_{\text{de},0}^s, \quad (22)$$

with  $m_{\text{de},0}^s = m_{\text{de}}^s(t=0)$ . Then one can write for the dielectric function  $\varepsilon(z) = \varepsilon_\infty + 4\pi\chi_{\text{de}}(z)$

$$\varepsilon(z) - \varepsilon_\infty = \frac{-4\pi\chi_{\text{de}}}{(z/\Omega_{\text{de}}^s)^2 - 1 - m_{\text{de},0}^s + \left[ iz\nu_{\text{de}}^s/\Omega_{\text{de}}^s{}^2 + \chi_{M,\text{de}}(z) \right]}. \quad (23a)$$

The inverse of the dielectric function,  $1/\varepsilon(z)$ , is occasionally considered as the dielectric modulus [30]. The exact Mori-Zwanzig representation, Eq. (21), suggests to rather consider  $[\varepsilon(z) - \varepsilon_\infty]^{-1}$ , i. e.  $\chi_{\text{de}}^{-1}(z)$ . This function consists of a quadratic polynomial in the frequency,  $(z/\Omega_{\text{de}}^s)^2 - 1 - m_{\text{de},0}^s$ , a white-noise background,  $iz\nu_{\text{de}}^s$ , and a non-trivial part  $\chi_{M,\text{de}}(z)$ . The latter has all the standard properties of a susceptibility, in particular it obeys Kramers-Kronig relations. There is the trivial relation between the spectrum  $\chi''_{M,\text{de}}(\omega)$  and the dielectric function

$$\text{Im} \left[ [\hat{\varepsilon} - \varepsilon(\omega)]^{-1} \right] = \frac{1}{4\pi\chi_{\text{de}}} \cdot \left[ \omega \left( \nu_{\text{de}}^s/\Omega_{\text{de}}^s{}^2 \right) + \chi''_{M,\text{de}}(\omega) \right]. \quad (23b)$$

Here,  $\varepsilon_\infty$  was replaced by the constant  $\hat{\varepsilon}$ , discussed above in connection with the fit of  $\varepsilon'(\omega)$ .

The full lines in Fig. 16 exhibit the right-hand side of Eq. (23b), evaluated with the model parameters used for the interpretation of the dielectric-loss spectra in Fig. 1. The symbols exhibit the left-hand side of Eq. (23b) calculated with the data from Ref. [6] and  $\hat{\varepsilon}$  determined in connection with the fits of  $\varepsilon'(\omega)$  in Fig. 8. Figure 16 shows that the fit is of equal quality as the ones shown for the direct analysis of the dielectric loss spectra.

However, to produce the result in Fig. 16, one has to be careful to subtract the right value of  $\hat{\varepsilon}$ . The error bars shown in the figure for  $T = 253$  K indicate the influence of subtracting  $\hat{\varepsilon} \pm 1$  instead of  $\hat{\varepsilon}$  to estimate the uncertainty introduced by this procedure. One notices that the shape of the curves for the high-frequency part is influenced. Thus an analysis based on  $[\hat{\varepsilon} - \varepsilon(\omega)]^{-1}$  is only practicable, if one can avoid these problems of the inversion procedure. Up to trivial terms, the left-hand side of Eq. (23b) is identical with the spectrum  $\omega m''_{\text{de}}(\omega)$  discussed in Fig. 14. This quantity can be explained well by the  $\beta$ -relaxation-scaling laws. Thus for PC, the corrections to the asymptotic laws are smaller for  $([\varepsilon(\omega) - \hat{\varepsilon}]^{-1})''$  than for  $\varepsilon''(\omega)$ . In particular it is shown by Fig. 15 that the square-root singularity can be identified from a discussion of  $\chi_{M,\text{de}}(\omega)$ .

## VII. CONCLUSION

It was exemplified for propylene carbonate as a typical glass-forming van-der-Waals system, that the susceptibility spectra measured by three different experimental techniques can be described well by a schematic MCT model. Several decades of intensity change in the GHz frequency window as seen in light-scattering and dielectric-loss experiments with a sensitive temperature dependence typical for glass-forming liquids are fitted. Also, the results from incoherent neutron scattering, probing the dynamics for different wave vectors could be included in this simultaneous fit. Real-part data from the dielectric experiment have been successfully analyzed as well to further corroborate the consistency of the schematic-model fit. For temperatures ranging from the critical value  $T_c \approx 180$  K to well above the melting point, the range of applicability of the model includes both  $\alpha$ - and  $\beta$ -relaxation windows, as well as the crossover to the microscopic spectrum. Below  $T_c$  and down to the glass-transition temperature  $T_g$ , a rather simple approach to account for hopping phenomena improves the fit for the  $\beta$ -minimum regime, but fails to describe the  $\alpha$ -peak below  $T_c$ .

The schematic model used in the fit captures the general features of the glass-transition scenario predicted by the full microscopic theory. Still, it allows to go further than an anal-

ysis based on the asymptotic predictions of MCT only. In particular, we have used the schematic model to investigate which features of the measured spectra can be described by asymptotic laws, and where preasymptotic corrections set in. We find that the asymptotic formulas qualitatively give an adequate description of the data. Thereby the preceding studies [1,3–7,10] are corroborated. But we demonstrated also, that preasymptotic-correction effects cause important quantitative differences between the data and the scaling-law results. One aspect of this is the  $T$ -drift of the critical amplitude  $h_{ls}^s$  noted in an earlier analysis of PC light-scattering data [1]. The drift of the coupling constant  $v_{ls}^s$  is not sufficient to explain this, as was demonstrated in Figs. 9 and 13. Also, the crossover to the microscopic excitations influences the height of the spectra at the  $\beta$  minimum. For the measurements analyzed, scaling works best with the neutron-scattering data, due to the relatively low plateau values  $f_q^{s,c}$ . An asymptotic analysis of the dielectric modulus could even work better in this respect. But due to uncertainties in the inversion of the dielectric function, such analysis is not practicable unless the modulus itself is measured directly.

## ACKNOWLEDGMENTS

We thank H. Z. Cummins, M. Fuchs, P. Lunkenheimer, M. R. Mayr, U. Schneider, A. P. Singh, and J. Wuttke for many helpful discussions and the authors of Ref. [1], Refs. [4–6], and Ref. [10] for providing us with their files for the various propylene-carbonate data. This work was supported by Verbundprojekt BMBF 03-G05TUM.

## REFERENCES

- [1] W. M. Du, G. Li, H. Z. Cummins, M. Fuchs, J. Toulouse, and L. A. Knauss, Phys. Rev. E **49**, 2192 (1994).
- [2] W. Götze and L. Sjögren, Rep. Prog. Phys. **55**, 241 (1992).
- [3] J. Ma, D. V. Bout, and M. Berg, Phys. Rev. E **54**, 2786 (1996).
- [4] P. Lunkenheimer, A. Pimenov, M. Dressel, B. Gorshunov, U. Schneider, B. Schiener, and A. Loidl, Am. Chem. Soc. Symp. Ser. **676**, 168 (1997).
- [5] P. Lunkenheimer, A. Pimenov, M. Dressel, B. Schiener, U. Schneider, and A. Loidl, Prog. Theor. Phys. Suppl. **126**, 123 (1997).
- [6] U. Schneider, P. Lunkenheimer, R. Brand, and A. Loidl, Phys. Rev. E **59**, 6924 (1999).
- [7] L. Börjesson, M. Elmroth, and L. M. Torell, Chem. Phys. **149**, 209 (1990).
- [8] M. Elmroth, L. Börjesson, and L. M. Torell, Phys. Rev. Lett. **68**, 79 (1992).
- [9] W. Götze, J. Phys.: Cond. Matt. **11**, A1 (1999).
- [10] J. Wuttke, M. Ohl, M. Goldammer, S. Roth, U. Schneider, P. Lunkenheimer, R. Kahn, B. Rufflé, and R. Lechner, Phys. Rev. E, 1999, submitted.
- [11] N. V. Surovtsev, J. A. H. Wiedersich, N. V. Novikov, E. Rössler, and A. P. Sokolov, Phys. Rev. B **58**, 14888 (1998).
- [12] H. C. Barshilia, G. Li, G. Q. Shen, and H. Z. Cummins, Phys. Rev. E **59**, 5625 (1999).
- [13] T. Franosch, M. Fuchs, W. Götze, M. R. Mayr, and A. P. Singh, Phys. Rev. E **55**, 7153 (1997).
- [14] M. Fuchs, W. Götze, and M. Mayr, Phys. Rev. E **58**, 3384 (1998).
- [15] U. Bengtzelius, W. Götze, and A. Sjölander, J. Phys. C **17**, 5915 (1984).

- [16] W. Götze and L. Sjögren, *Z. Phys. B* **65**, 415 (1987).
- [17] F. Sciortino and P. Tartaglia, *J. Phys.: Cond. Matt.* **11**, A261 (1999).
- [18] C. Alba-Simionescu and M. Krauzman, *J. Chem. Phys.* **102**, 6574 (1995).
- [19] C. Alba-Simionescu, V. Krakoviack, M. Krauzman, P. Migliardo, and F. Romain, *J. Ram. Spect.* **27**, 715 (1996).
- [20] V. Krakoviack, C. Alba-Simionescu, and M. Krauzman, *J. Chem. Phys.* **107**, 3417 (1997).
- [21] W. Götze, *Z. Phys. B* **56**, 139 (1984).
- [22] L. Sjögren, *Phys. Rev. A* **33**, 1254 (1986).
- [23] T. Franosch, M. Fuchs, W. Götze, M. R. Mayr, and A. P. Singh, *Phys. Rev. E* **56**, 5659 (1997).
- [24] T. Franosch, W. Götze, M. R. Mayr, and A. P. Singh, *Phys. Rev. E* **55**, 3183 (1997).
- [25] A. P. Singh, G. Li, W. Götze, M. Fuchs, T. Franosch, and H. Z. Cummins, *J. Non-Cryst. Solids* **235–237**, 66 (1998).
- [26] B. Rufflé, C. Ecolivet, and B. Toudic, *Europhys. Lett.* **45**, 591 (1999).
- [27] W. Götze, in *Liquids, Freezing and Glass Transition*, edited by J. P. Hansen, D. Levesque, and J. Zinn-Justin (North-Holland, Amsterdam, 1991), pp. 287–503.
- [28] M. Fuchs, W. Götze, S. Hildebrand, and A. Latz, *J. Phys.: Cond. Matt.* **4**, 7709 (1992).
- [29] T. Franosch, W. Götze, M. R. Mayr, and A. P. Singh, *J. Non-Cryst. Solids* **235–237**, 71 (1998).
- [30] P. B. Macedo, C. T. Moynihan, and R. Bose, *Phys. Chem. Glasses* **13**, 171 (1972).

## FIGURES

FIG. 1. Susceptibility spectra for propylene carbonate (PC,  $T_m \approx 218\text{ K}$ ,  $T_g = 160\text{ K}$ ) as measured by depolarized-light-scattering (upper panel, data from Ref. [1]), and dielectric-loss spectroscopy (lower panel, data from Ref. [6]), normalized with a temperature-independent static susceptibility. Temperatures are in steps of 10 K, unless indicated otherwise; in the dielectric measurement,  $T = 243, 263, 273, 283\text{ K}$  are missing, for the light-scattering experiment, the highest temperature is 250 K (see text for details). The full lines are fits by solutions of the two-component schematic MCT model defined in Sec. II with parameters as described in the text. The dashed lines indicate a white-noise spectrum,  $\chi''_{\text{wh.n.}}(\omega) \propto \omega$ ; the dash-dotted line in the upper panel exhibits the asymptote of the critical spectrum  $\chi''(\omega) \propto \omega^a$  according to Eq. (15), with  $a = 0.30$  corresponding to the value of  $\lambda = 0.75$ . The dotted line shows the solution of the model for  $T = T_c$  and hopping terms neglected.

FIG. 2. Susceptibility spectra for PC as measured by incoherent neutron scattering for three wave vectors  $q$ , from Ref. [10]. Temperatures are  $T = 210, 220, 230, 240, 251, 260, 285\text{ K}$ , where alternating open and filled symbols have been used to help distinguishing different data sets. For lower temperatures, data points below 10 GHz are seriously affected by the spectrometer's resolution function and therefore not shown. Full lines are fits as in Fig. 1.

FIG. 3. Vertices  $v_1, v_2$  for the first mode-coupling functional, Eq. (3b), used for the fits shown in Figs. 1 and 2. In the above diagram, the thick line represents the curve of glass-transition singularities, Eq. (4), while the thin line serves as a guide to the eye indicating the chosen path. Each dot corresponds to one temperature. The lower diagram shows the separation parameter  $\sigma$ , Eq. (8), as a function of  $T$ ; the critical temperature  $T_c \approx 180\text{ K}$  is determined from the zero of the shown regression line.

FIG. 4. (a) Coupling coefficients  $v_A^s$  for the second mode-coupling functional, Eq. (5b), used for the fits shown in Figs. 1 and 2 as functions of temperature. The squares refer to the light-scattering data and the circles to the dielectric-loss spectra; the lines through the symbols are guides to the eye. The lines without symbols connect the  $v_{\text{ns}}^s(q)$  used for the neutron-scattering data for 10 wave vectors  $q = 0.5, 0.6, \dots, 1.4 \text{ \AA}^{-1}$  (from top to bottom). The vertical dashed line indicates the critical temperature  $T_c$ . (b) Coefficients  $v_{\text{ns}}^s(q, T)$  for the neutron-scattering data as functions of  $q$  for various fixed  $T$ . From top to bottom, the temperatures increase from  $T = 210 \text{ K}$  to  $285 \text{ K}$  (as given in Fig. 2). The dashed lines indicate  $A/q + B/q^2$  laws to visualize the difference to a  $1/q$ -law behavior, which is shown as a dot-dashed line; see text for details.

FIG. 5. Oscillator frequencies  $\Omega_A^s$  and damping constants  $\nu_A^s$  in THz specifying the transient motion for the second correlator as functions of temperature as used for the fits shown in Figs. 1 and 2. The squares refer to the light-scattering spectra, circles to the dielectric loss spectra; lines through the symbols are guides to the eye. For the neutron-scattering spectra,  $\nu_{\text{ns}}^s$  was taken  $q$ -independent (diamonds in the lower panel), and the  $\Omega_{\text{ns}}^s$  exhibit the  $q \cdot \sqrt{T}$ -behavior shown in the upper panel (lines without symbols,  $q$  range as in Fig. 4). The vertical dashed lines indicate the critical temperature  $T_c$ .

FIG. 6. In the upper part, the hopping coefficient  $\Delta$  entering Eq. (3a) for the first correlator used for the fits shown in Fig. 1 to the dielectric (circles) and light-scattering (squares) data is exhibited. The values follow an Arrhenius-type temperature dependence, indicated by a straight line. For the fit to the neutron-scattering data, the same values could be used, but show no influence on the fit curves in Fig. 2 (see text for details). For the fit to the dielectric data, an additional hopping coefficient  $\Delta_{\text{de}}^s$  for the second correlator had to be used, shown by the circles in the lower part of this figure; here, the values  $(\Omega_{\text{de}}^s/\Omega)^2 \Delta_{\text{de}}^s$  follow an Arrhenius law indicated by a straight line. The vertical dashed line indicates  $1000/T_c$  with  $T_c = 180 \text{ K}$ .

FIG. 7. The solid lines reproduce the susceptibility spectra  $\chi''_A(\omega)$  from Fig. 1 used for the fit to the light-scattering (upper panel) and the dielectric-loss spectra (lower panel), respectively. Dashed lines are solutions using the same model parameters, but with hopping effects ignored:  $\Delta = \Delta_{\text{de}}^s = 0$ . Notice that the dashed lines for temperatures  $T$  below  $T_c$  exhibit a “knee” which is located between 10 and 100 GHz and moves to higher frequencies with decreasing  $T$ .

FIG. 8. Measured values for the real part  $\varepsilon'(\omega)$  of the dielectric function from Ref. [6] for  $T = 173\text{ K}$  through  $T = 233\text{ K}$  in steps of  $10\text{ K}$ , and for  $T = 253\text{ K}$  (from left to right). Experimental data have been shifted by  $\hat{\varepsilon}$  to account for an unknown background; see text for details. Temperatures  $T = 163\text{ K}$  and below, and  $T = 293\text{ K}$  are not shown in order to avoid overcrowding of the figure. For the same reason, the data points for frequencies above 1 GHz have been partially removed for all but the highest temperature and are only shown in the inset. The full lines are the real parts of the calculated susceptibilities for the same model parameters as used for the curves in Fig. 1.

FIG. 9. The full lines show  $\hat{\phi}_x(t) = (\phi_x(t) - f_x^c)/h_x$  for times where  $\hat{\phi}_x(t) > 0$ . The dash-dotted straight lines exhibit  $(t/t_0)^{-a}$ , with  $t_0 = 0.035\text{ ps}$  and  $a = 0.30$ . The dashed lines show the  $\beta$ -correlators  $G(t)$  for the indicated temperatures (see text). The uppermost set of curves refers to the first correlator of the schematic model. The other two sets refer to the light-scattering and the dielectric response studied in Fig. 1. The sets are shifted vertically by one (light scattering), respectively two (dielectric response) decades for clarity.

FIG. 10. Effective nonergodicity parameters determined from the calculated  $\phi_x$ -versus- $\log t$  curves for the spectra shown in Fig. 1:  $f(T)$  for the first correlator  $\phi(t)$  (open circles), and  $f_A^s(T)$  for the correlators  $\phi_{ls}^s(t)$  and  $\phi_{de}^s(t)$  (filled squares and circles, respectively). The solid lines exhibit the leading-order-asymptotic laws for  $f_x$  from Eq. (17) for  $T \leq T_c$  and  $f_x^c$  for  $T \geq T_c$ . The vertical dashed line indicates the crossover temperature  $T_c = 180$  K. The crosses in the lowest panel are estimations of  $f_{de}^s$  obtained in Ref. [6] by fitting the measured  $\varepsilon'(\omega)$  data with a Cole-Davidson function. The dashed lines through the solid symbols connect the values calculated from Eq. (18b) (see text for details).

FIG. 11. The upper part of the figure (scale on right axis) shows the rescaled susceptibility spectra for four temperatures for the first correlator of the schematic model,  $\omega\phi''(\omega)/h\sqrt{|\sigma|}$ , as a function of  $\hat{\omega} = \omega t_\sigma$ . Hopping terms have been set to zero. The lower part (scale on the left axis) shows the  $\omega\phi_A^{s''}(\omega)/h_A\sqrt{|\sigma|}$ -versus- $\hat{\omega}$  curves for  $T = 210$  K for the light-scattering (line with squares) and neutron-scattering correlators at  $q = 1.0 \text{ \AA}^{-1}$  and  $q = 1.1 \text{ \AA}^{-1}$  (lines), and for  $T = 213$  K for the dielectric correlators (line with circles). The dashed lines indicate the master spectrum for  $\lambda = 0.75$  with the minimum position  $(\hat{\omega}_{\min}, \hat{\chi}_{\min})$  marked by a diamond.

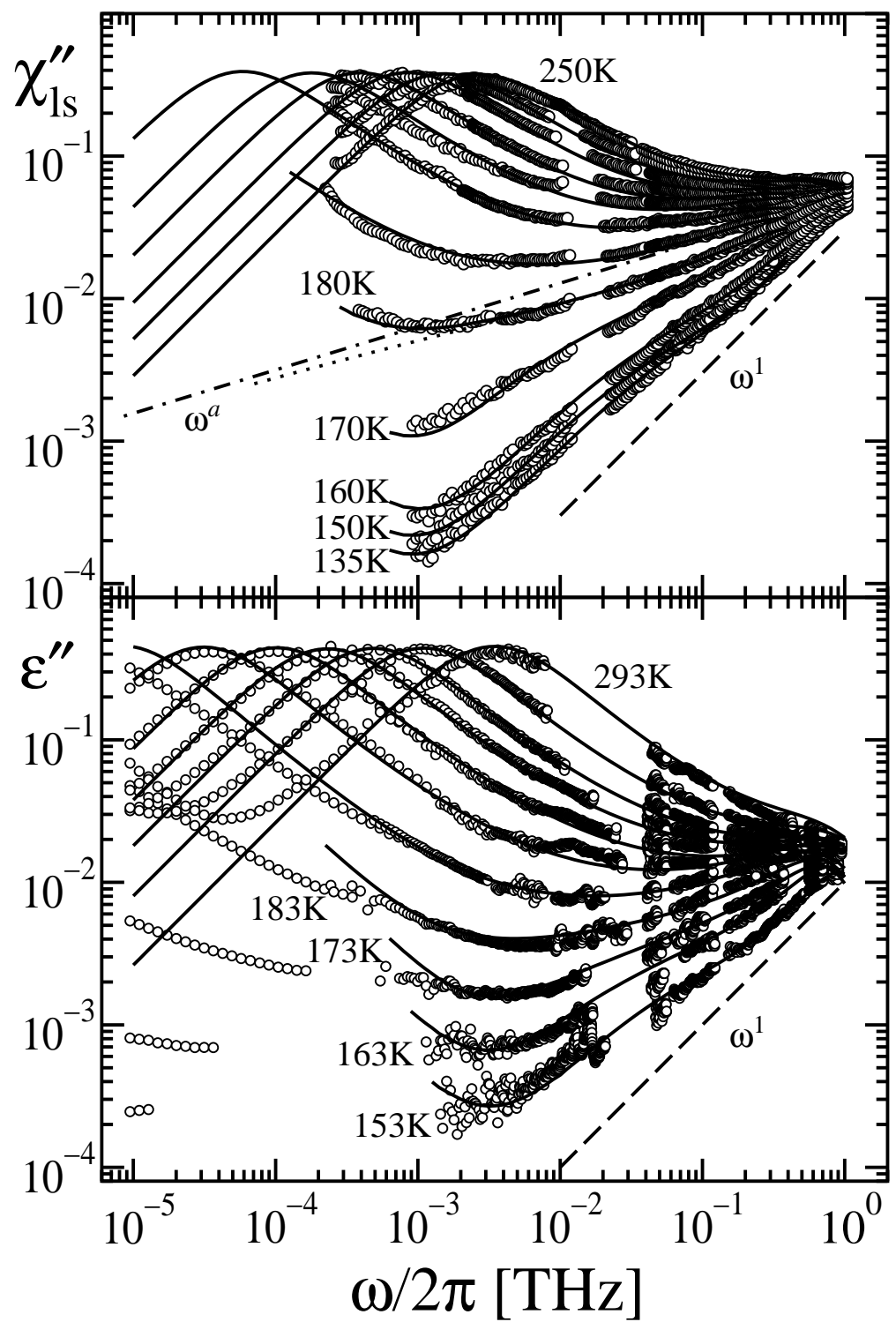
FIG. 12. Rectification diagram for the minimum positions  $\omega_{\min}$  of the dielectric-loss (circles), light-scattering (squares), and neutron-scattering (triangles) fit. The neutron-scattering data have been averaged over the investigated  $q$  range, and error bars indicate the smallest and highest values. The vertical dashed line marks the critical point  $T_c$ . The solid line is the asymptotic-formula result for the minimum positions calculated from the  $\beta$ -relaxation-scaling law for the fit parameters of the model used in Figs. 1 and 2. The dashed lines show the linear interpolation through the data points, restricted to the regime  $190 \text{ K} \leq T \leq 250 \text{ K}$ , for the dielectric-loss and for the light-scattering data, respectively.

FIG. 13. Scaling-law analysis of the MCT solutions shown in Fig. 1 for the fit of the light-scattering spectra. The lower set of curves shows the rescaled spectra  $\chi''_{ls}(\omega)/h_{ls}\sqrt{|\sigma|}$  for  $T = 220, 210, 200, 190 (from top to bottom). The upper set of curves shows the same spectra, but now rescaled with  $h_{ls}$  replaced by the effective amplitude  $h_{ls}^{\text{eff}}$  from Eq. (18b). Notice that the order of the rescaled spectra is now inverted. The asymptotic result  $\hat{\chi}$  is plotted as a dashed line with the minimum position marked by a diamond. The result for  $T = 180$  K with hopping effects ignored is added to demonstrate the approach towards the scaling limit.$

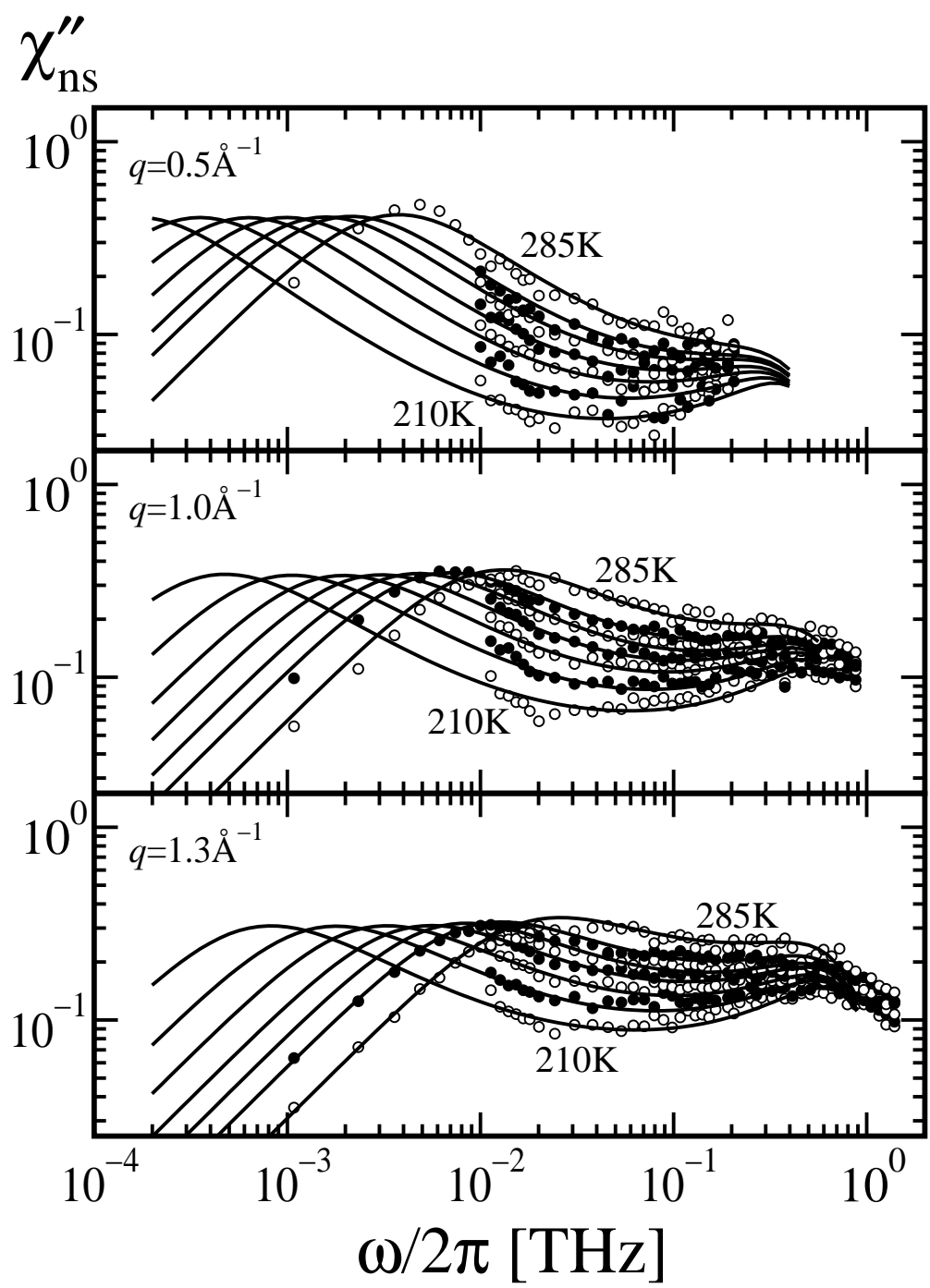
FIG. 14. Scaling-law analysis of the spectra for the memory kernel from the MCT solutions shown in Fig. 1 to interpret the dielectric function. The upper set of solid curves shows the unnormalized rescaled spectra,  $-\omega m''_{de}(\omega)/\sqrt{|\sigma|}$ , for temperatures  $T = 193, 203, 213$  K. In the lower part of the figure, the scaling is shown for the normalized rescaled spectra  $-\omega \hat{m}''_{de}(\omega)/\sqrt{|\sigma|}$  (see text for details). The dashed lines are the master spectra, with the minimum positions marked by diamonds.

FIG. 15. (a) Unnormalized nonergodicity parameters  $f_{M,de}^s$  for the memory kernel from the fit to the dielectric spectra (open circles). The asymptotic prediction is plotted as a solid line, the vertical dashed line indicates  $T_c$ . (b) Same as in (a), but normalized values  $\hat{f}_{M,de}^s$  (filled circles). The dash-dotted line indicates the critical plateau value for the first correlator of the schematic model,  $f^c$ .

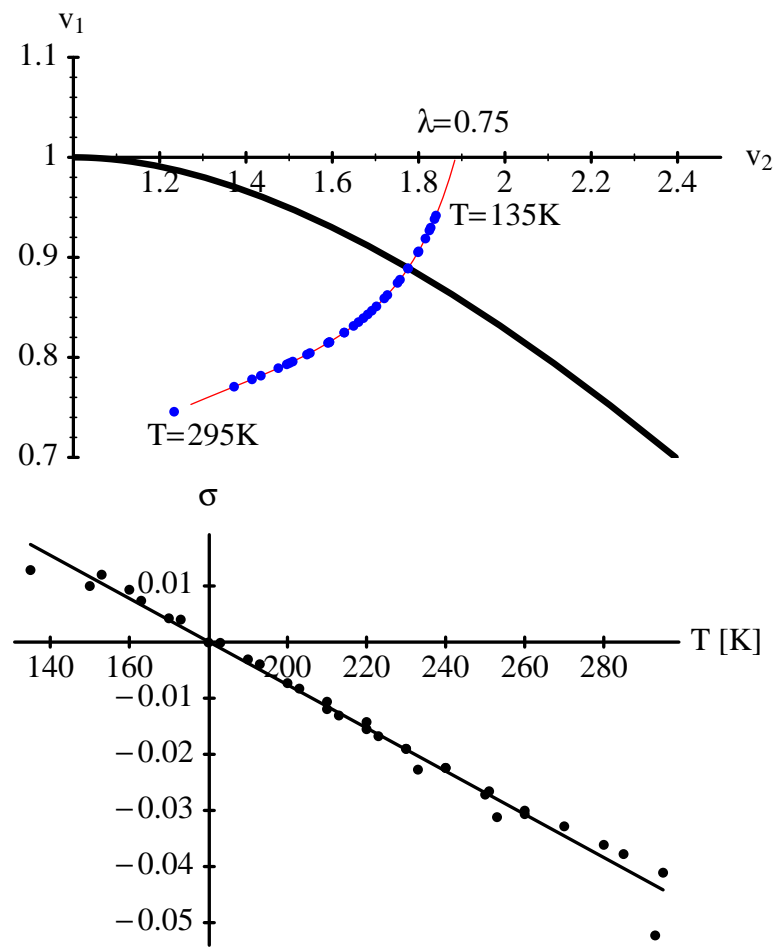
FIG. 16. The lines show the dielectric-modulus spectra defined by the right-hand side of Eq. (23b). The circles exhibit  $\text{Im} [\hat{\varepsilon} - \varepsilon(\omega)]^{-1}$  calculated from the dielectric-function data of Ref. [6]. The curves and the data sets have been shifted vertically to avoid overlapping; temperatures and shift factors are (183 K, 1), (193 K, 0.316), (203 K, 0.1), (213 K, 0.0316), (223 K, 0.01), (233 K, 0.00316), (253 K, 0.001). For the highest temperature, an estimation of the uncertainty introduced by inverting the experimental data is given as error bars; see text for details.



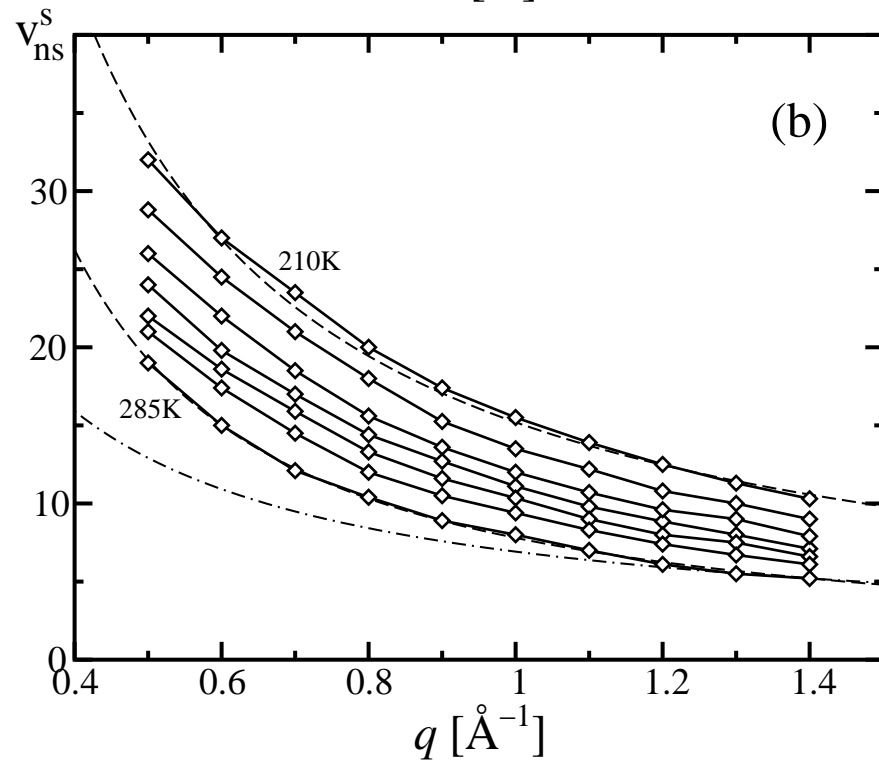
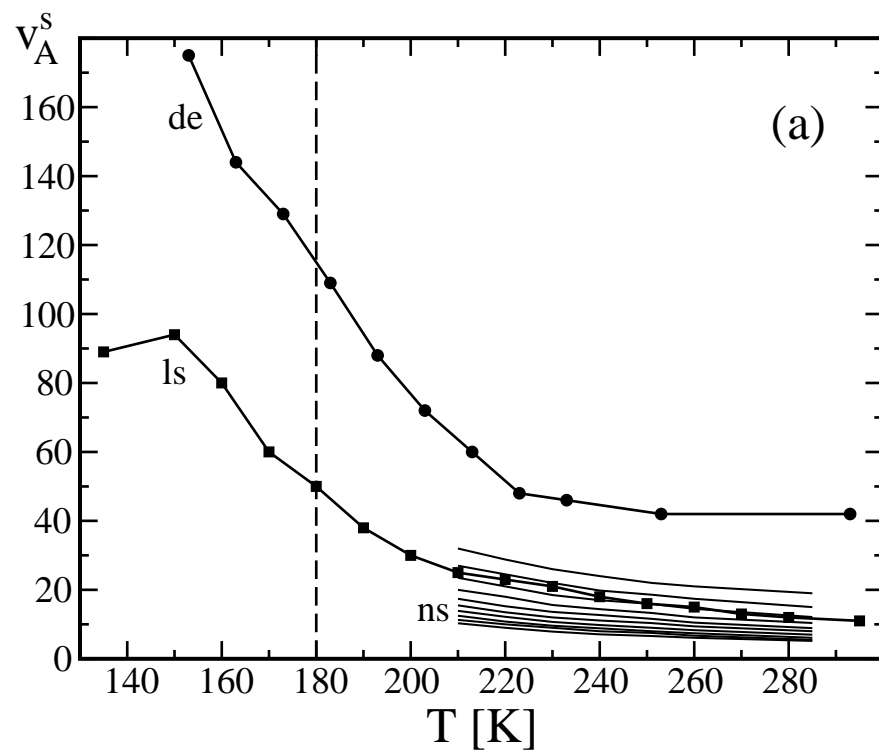
Götze and Voigtmann Figure 1



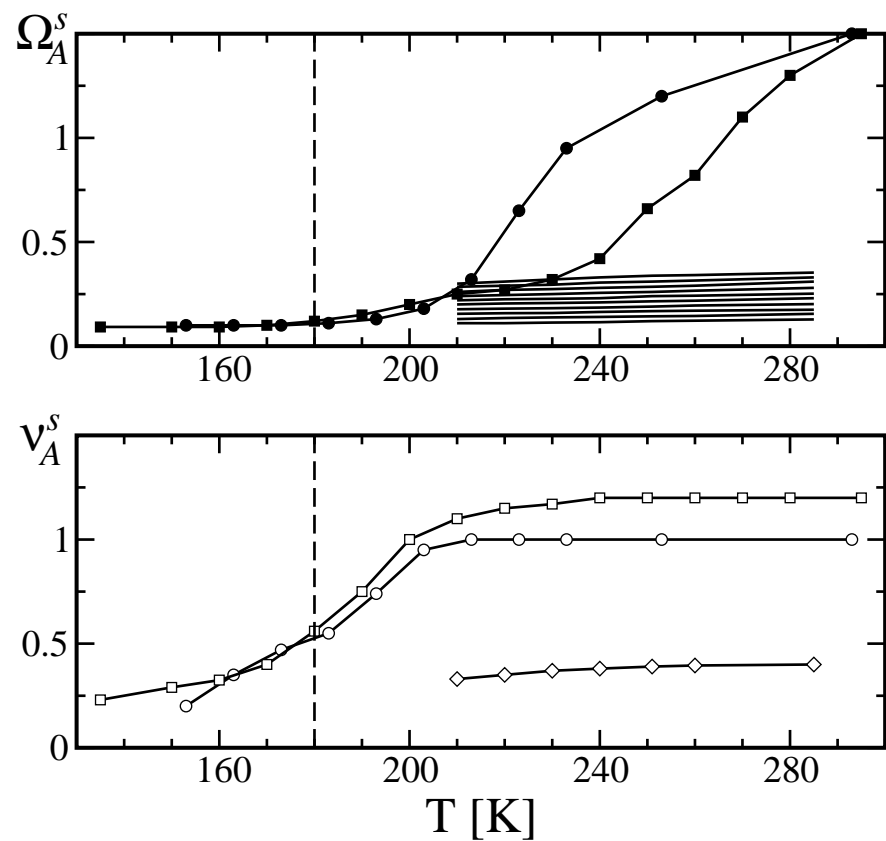
Götze and Voigtmann Figure 2



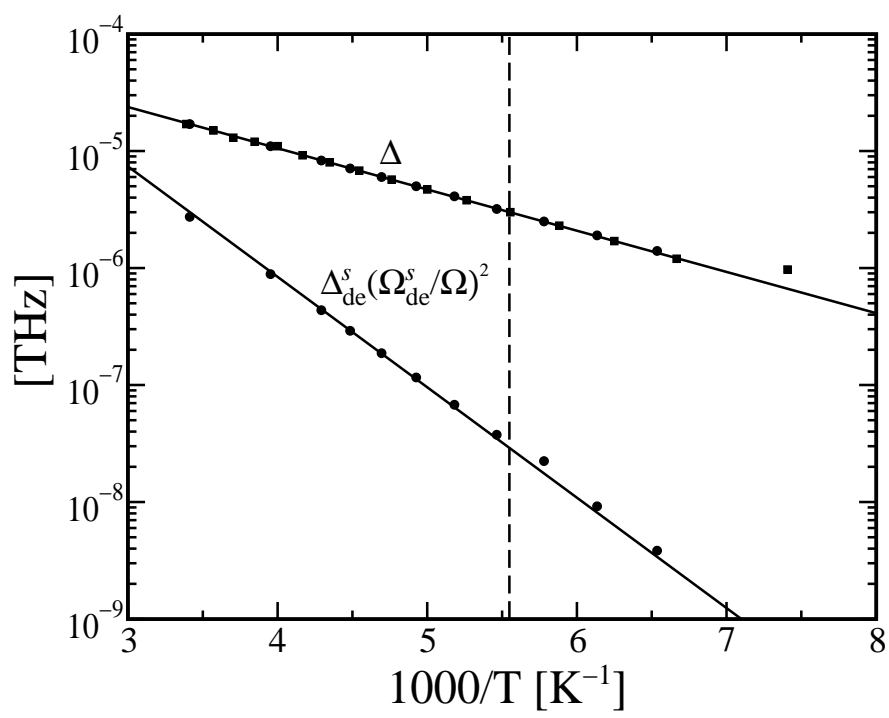
Götze and Voigtmann Figure 3



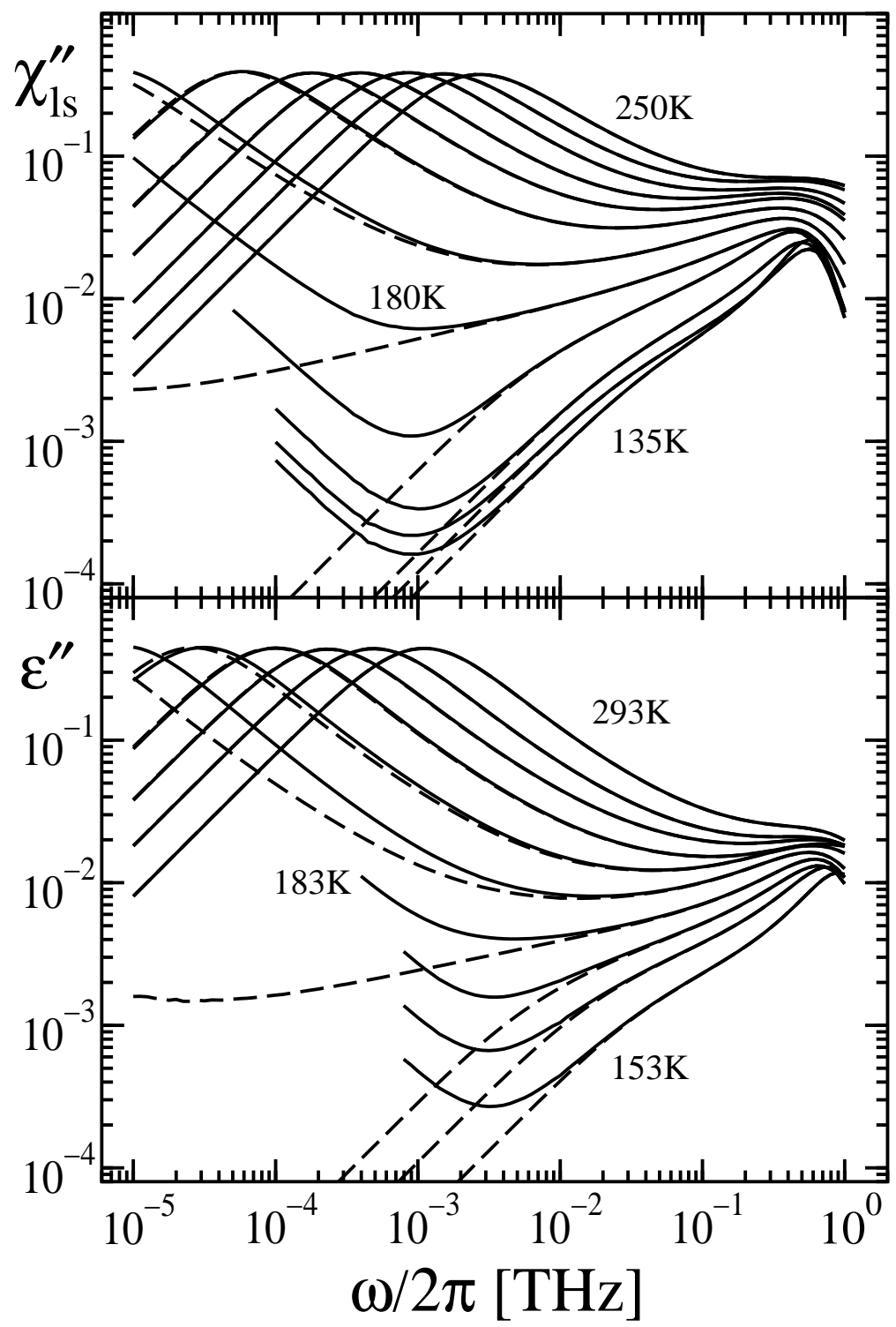
Götze and Voigtmann Figure 4



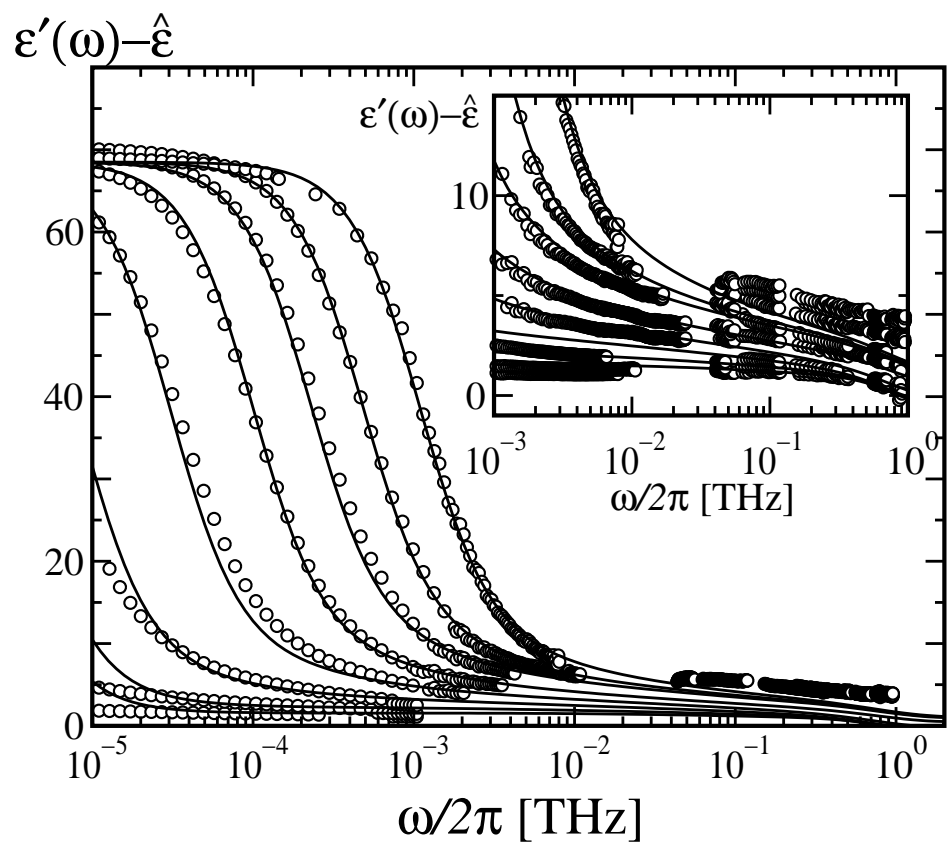
Götze and Voigtmann Figure 5



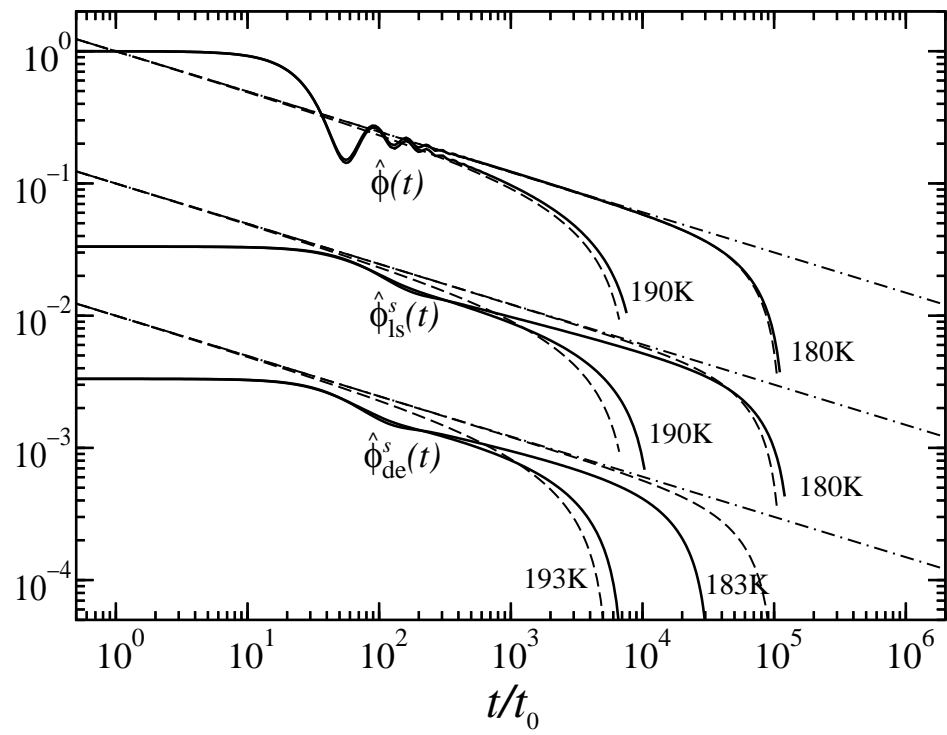
Götze and Voigtmann Figure 6



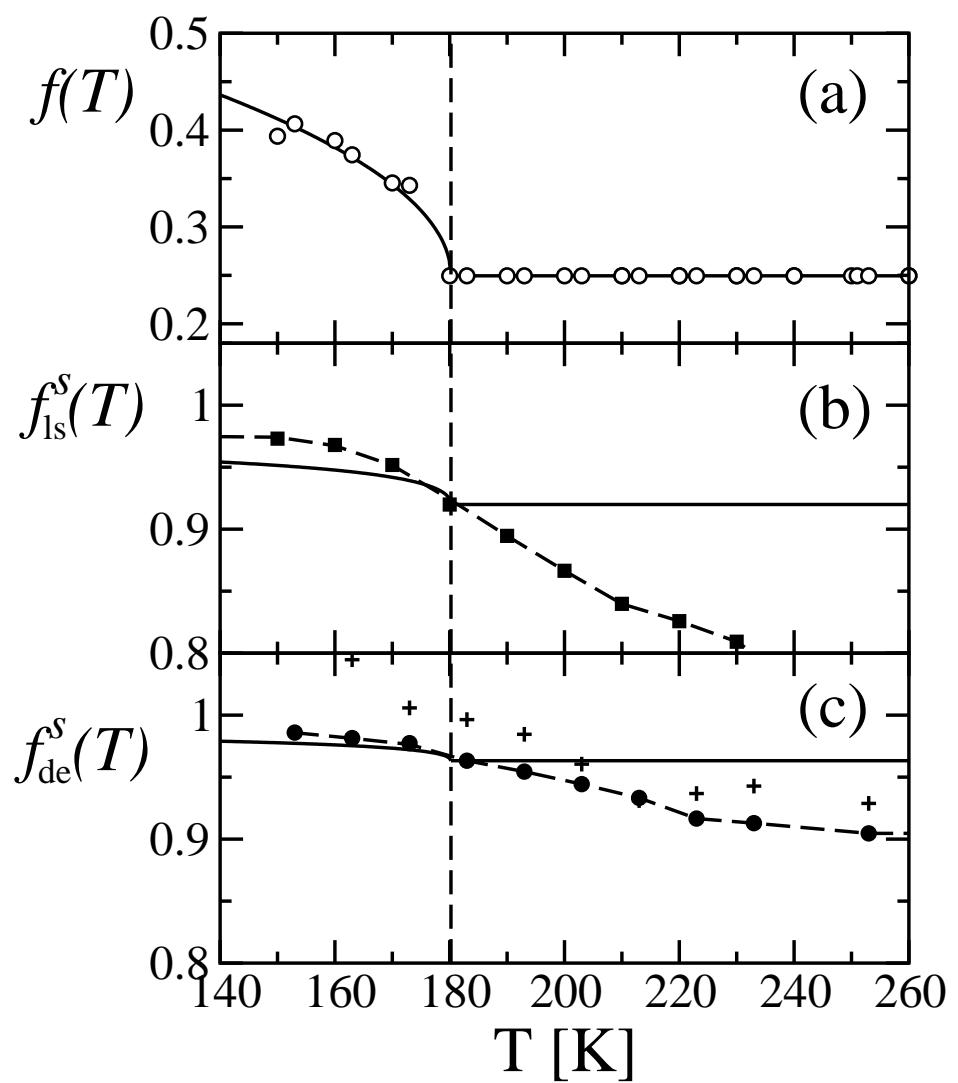
Götze and Voigtmann Figure 7



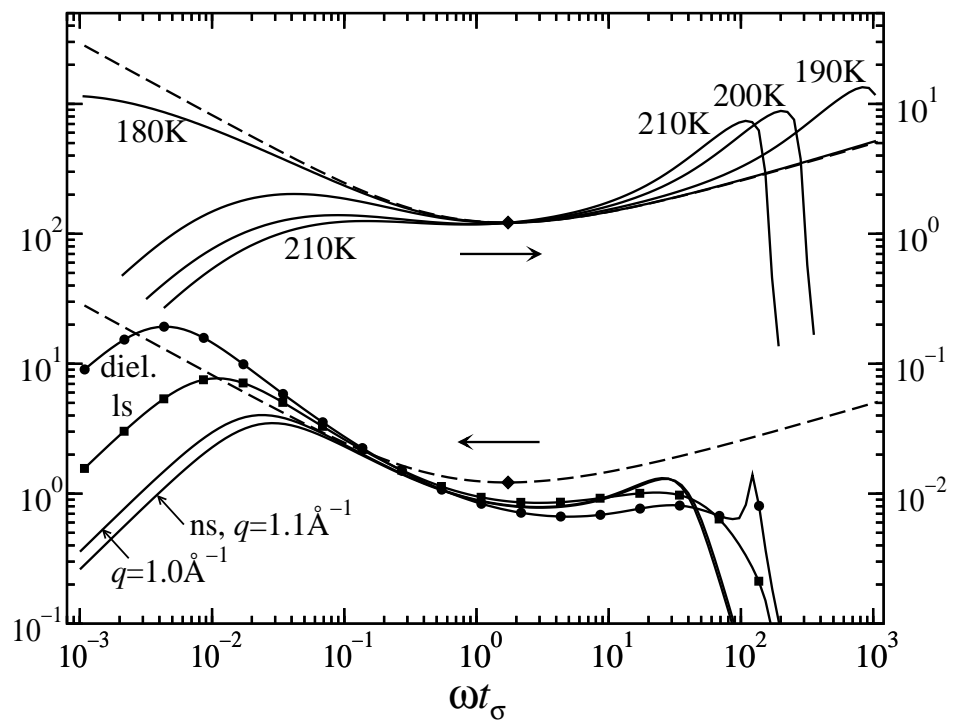
Götze and Voigtmann Figure 8



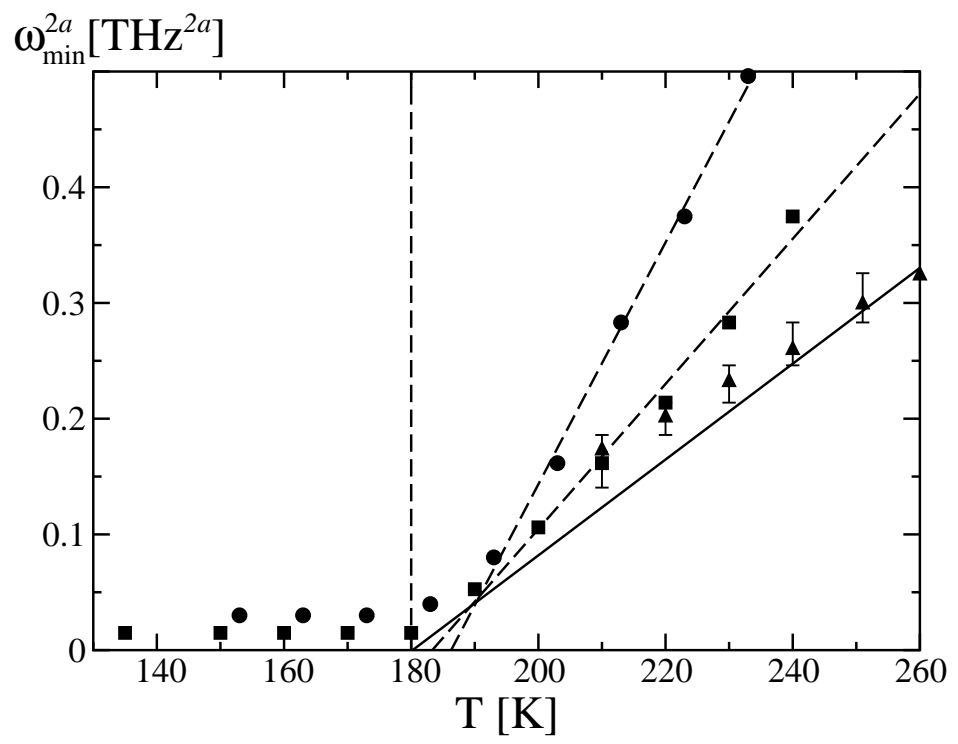
Götze and Voigtmann Figure 9



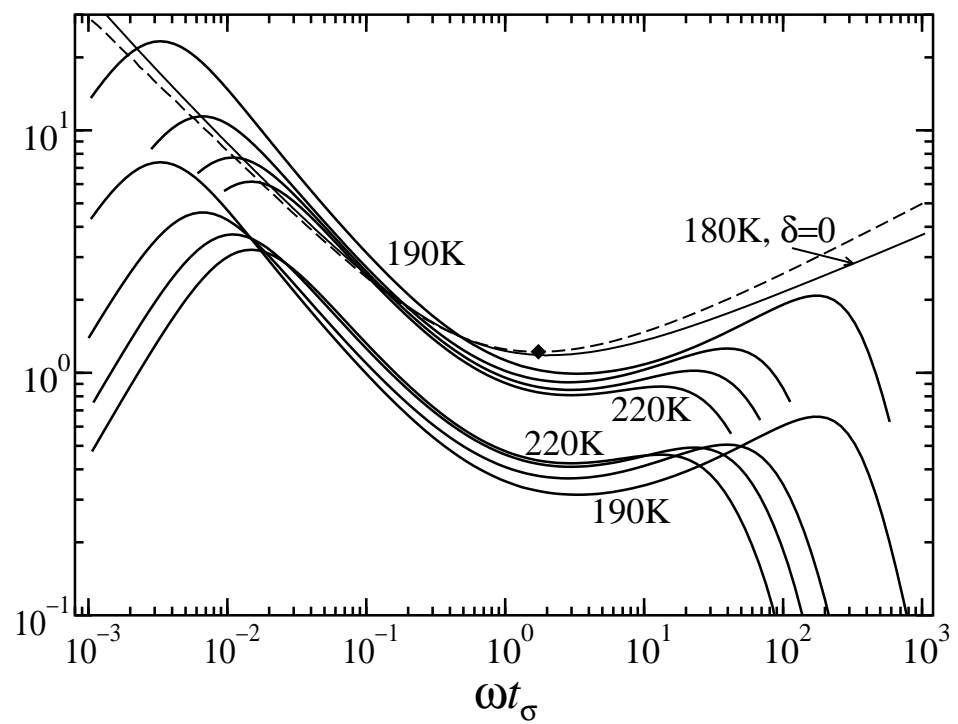
Götze and Voigtmann Figure 10



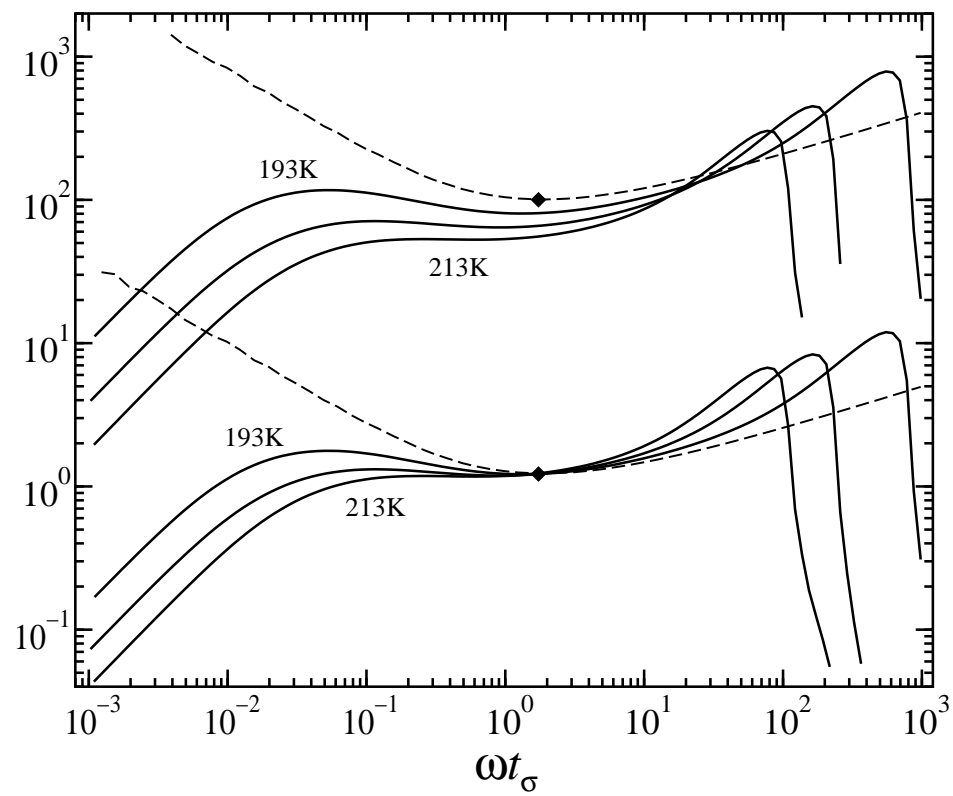
Götze and Voigtmann Figure 11



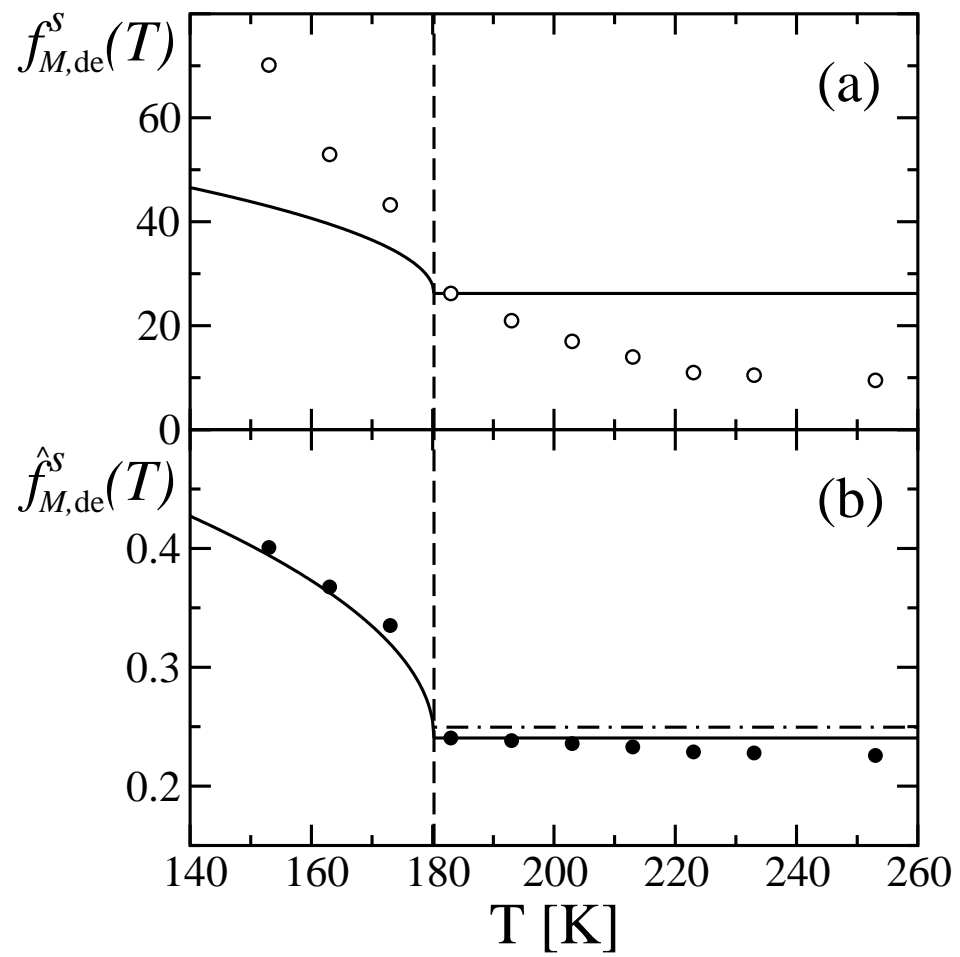
Götze and Voigtmann Figure 12



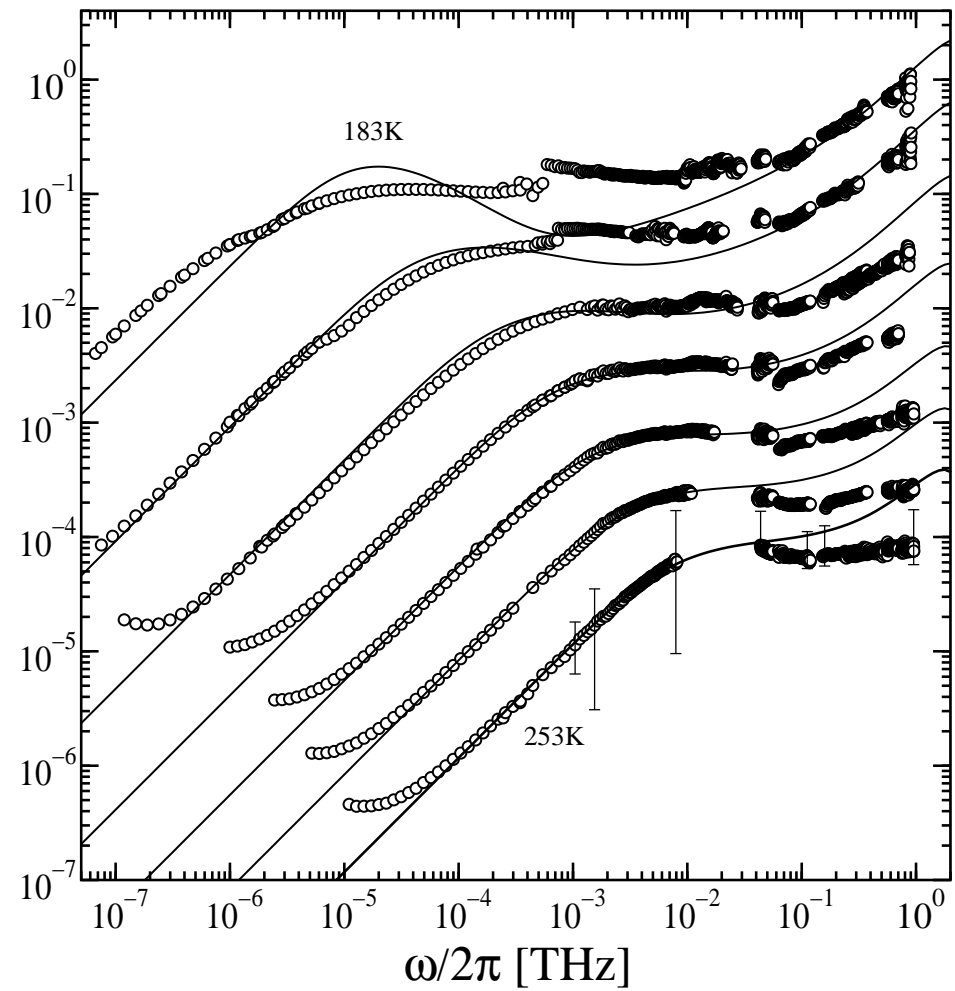
Götze and Voigtmann Figure 13



Götze and Voigtmann Figure 14



Götze and Voigtmann Figure 15



Götze and Voigtmann Figure 16